arXiv:1704.03234v1 [cs.IT] 11 Apr 2017

Error Bounds for Uplink and Downlink 3D Localization in 5G mmWave Systems

Zohair Abu-Shaban, *Student Member, IEEE*, Xiangyun Zhou, *Member, IEEE*, Thushara Abhayapala, *Senior Member, IEEE*, Gonzalo Seco-Granados, *Senior Member, IEEE*, and Henk Wymeersch, *Member, IEEE*,

Abstract

Location-aware communication systems are expected to play a pivotal part in the next generation of mobile communication networks. Therefore, there is a need to understand the localization limits in these networks, particularly, using millimeter-wave technology (mmWave). Towards that, we address the uplink and downlink localization limits in terms of 3D position and orientation error bounds for mmWave multipath channels. We also carry out a detailed analysis of the dependence of the bounds of different systems parameters. Our key findings indicate that the uplink and downlink behave differently in two distinct ways. First of all, the error bounds have different scaling factors with respect to the number of antennas in the uplink and downlink. Secondly, uplink localization is sensitive to the orientation angle of the user equipment (UE), whereas downlink is not. Moreover, in the considered outdoor scenarios, the non-line-of-sight paths generally improve localization when a line-of-sight path exists. Finally, our numerical results show that mmWave systems are capable of localizing a UE with sub-meter position error, and sub-degree orientation error.

I. Introduction

A strong candidate for the fifth generation of mobile communication (5G) is millimeter-wave (mmWave) multiple-input-multiple-output (MIMO) technology, where both the user equipment (UE) and the base station (BS) are equipped with arrays of large number of antennas, and operate at a carrier frequency in the range of 30–300 GHz [1]–[5]. Location-aided systems are expected

Zohair Abu-Shaban, Xiangyun Zhou, and Thushara Abhayapala are with the Research School of Engineering (RSEng), the Australian National University (ANU), Canberra, Australia. Emails: {zohair.abushaban, xiangyun.zhou, thushara.abhayapala}@anu.edu.au. Henk Wymeersch is with the Department of Signals and Systems, Chalmers University of Technology, Sweden. Email: henkw@chalmers.se. Gonzalo Seco-Granados is with the Department of Telecommunications and Systems Engineering, Universitat Autònoma de Barcelona, Spain (UAB). Email: gonzalo.seco@uab.es.

This work is partly supported by the Horizon2020 project HIGHTS (High precision positioning for cooperative ITS applications) MG-3.5a-2014-636537, the VINNOVA COPPLAR project, funded under Strategic Vehicle Research and Innovation Grant No. 2015-04849, the Australian Research Council's Discovery Projects funding scheme under Project DP140101133, and the Spanish Grant TEC2014-53656-R.

to have a wide range of applications in 5G mmWave communication [6], whether for vehicular communications [7], assisted living applications [8], or to support the communication robustness and effectiveness in different aspects such as resource allocation [9], beamforming [10], [11], and pilot assignment [12]. Therefore, the study of positioning in 5G mmWave systems becomes specially imperative. Due to the use of directional beamforming in mmWave, in addition to the UE position also the UE *orientation* plays an important role in location-aided systems.

Conventionally position information is obtained by GPS, though this has several limitations. Most importantly, GPS suffers from degraded performance in outdoor rich-scattering scenarios and urban canyons, and may fail to provide a position fix for indoor scenarios. Even in good conditions, GPS positioning accuracy ranges between 1–5 meters. To address these limitations, there has been intense research on competing radio-based localization technologies. To understand the fundamental behavior of any technology, the Cramér-Rao lower bound (CRLB)[13] or related bounds can be used. The CRLB provides a lower bound on the variance of an unbiased estimator of a certain parameter. The square-root of the CRLB of the position and the orientation are termed the position error bound (PEB), and the orientation error bound (OEB), respectively. PEB and OEB can be computed indirectly by transforming the bounds of the channel parameters, namely: directions of arrival (DOA), directions of departure (DOD), and time of arrival (TOA).

For conventional MIMO systems, the bounds of the 2D channel parameters are derived in [14], based on received digital signals and uniform linear arrays (ULA), while bounds are derived in [15] based on 3D channel matrix with no transmit beamforming. It was found that having more transmit and receive antennas is beneficial for estimating the DOA and DOD. In both [14], [15] beamforming was not considered. The bounds on the channel parameters can be transformed into PEB and OEB as in [16]–[19] that considered 2D cooperative wideband localization, highlighting the benefit of large bandwidths.

MmWave communication combines large antenna arrays with large bandwidths, and should be promising for localization, then. In [20], PEB and OEB for 2D mmWave downlink localization using ULA are reported, while [21] considers 2D uplink multi-anchor localization. Furthermore, for indoor scenarios, PEB and OEB are analyzed in [22] for 3D mmWave uplink localization with a single beam whose direction is assumed to be known. Multipath environments are considered in the works in [20]–[22]. However, the difference between the uplink and downlink for 3D and 2D with large number of antennas and analog transmit beamforming is yet to be investigated.

In this paper, we consider 3D mmWave localization problem for both the uplink and downlink

under multipath conditions, and derive and analyze the PEB and OEB using multi-beam directional beamforming with arbitrary array geometry. We derive these bounds by transforming the Fisher information matrix (FIM) of the channel parameters into the FIM of location parameters. We stress that although the FIM of the channel parameters is symmetric in the uplink and downlink, this is untrue for the location parameters FIM, which leads the uplink and downlink to have different PEB and OEB. The contributions of this paper are summarized as follows:

- We show that, under some conditions, the multipath parameter estimation problem can be reduced to a problem of multiple single-path estimation. We refer to this reduction as the approximate approach.
- We derive the single-path CRLB of the channel parameters in a closed-form for arbitrary geometry, and show how these bounds are related to the PEB and OEB bounds. We also propose closed-form expressions of PEB and OEB for 3D and 2D line-of-sight (LOS) localization.
- We derive the PEB and OEB for general uplink and downlink localization, based on exact and approximate approaches, and show the asymmetry between uplink and downlink via both analytical scaling results and Monte-Carlo simulations with a uniform rectangular array (URA).

The rest of this paper is organized as follows. Section II presents the problem statement. Then, in Section III, we derive the FIM of the channel parameters in a general setup of arbitrary arrays for 3D localization, which we then specify for URA and ULA. The transformation of the channel parameters FIM into PEB and OEB is detailed in Section IV. The simulation results and the related insights are provided in Section V. Finally, the conclusions are reported in Section VI.

II. Problem Formulation

A. System Geometry

We consider a BS equipped with an array of N_{BS} antennas arranged in an arbitrary but known geometry whose centroid is located at the origin ($\mathbf{O}$), and orientation angle is $\mathbf{o}_{\mathrm{BS}} = [0, 0]^{\mathrm{T}}$. On the other hand, the centroid of the UE is located at an unknown position $\mathbf{p} = [p_x, p_y, p_z]^{\mathrm{T}}$ and equipped with a second array of N_{UE} antennas arranged in an arbitrary but known geometry with an unknown orientation $\mathbf{o} = [\theta_0, \phi_0]^{\mathrm{T}}$. An example with URAs is depicted in Fig. 1. There are $M \geq 1$ paths between BS and UE, where the first path is LOS, while with the other $M-1$ paths are associated with clusters located at $\mathbf{q}_m = [q_{m,x}, q_{m,y}, q_{m,z}]^{\mathrm{T}}$, $2 \leq m \leq M$. These clusters can reflectors or scatterers. Due to the mmWave propagation characteristics, the number of paths is small [2] and correspond to single-bounce reflections [20], [23]. Thus, the channel can be

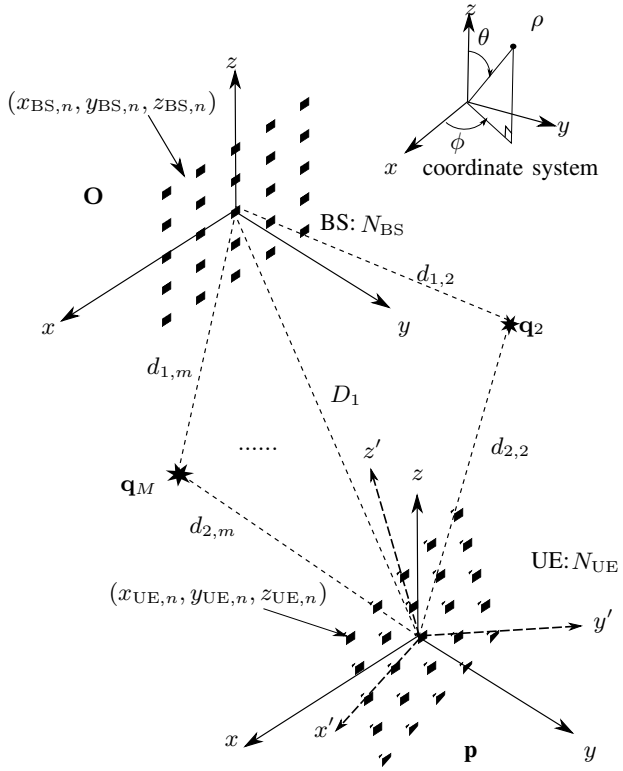

Fig. 1. An example scenario composed of a URA of $N_{\mathrm{UE}} = N_{\mathrm{BS}} = 25$ antennas, and M paths. We use the spherical coordinate system highlighted in the top right corner. The axes rotated by orientation angles (θ_0, ϕ_0) are labeled x', y', z'.

considered spatially sparse, and the parameters of different paths are assumed to be distinct, i.e., we assume unique DOAs, DODs TOA, and channel gains.

B. Channel Model

Denote[1] the m^{th} DOD and DOA by $(\theta_{\mathrm{T},m}, \phi_{\mathrm{T},m})$ and $(\theta_{\mathrm{R},m}, \phi_{\mathrm{R},m}), 1 \leq m \leq M$, respectively, where the related unit-norm array response vectors are given by [24]

$$\mathbf{a}_{\mathrm{T},m}(\theta_{\mathrm{T},m}, \phi_{\mathrm{T},m}) \triangleq \frac{1}{\sqrt{N_{\mathrm{T}}}} e^{-j\boldsymbol{\Delta}_{\mathrm{T}}^{\mathrm{T}}\mathbf{k}(\theta_{\mathrm{T},m}, \phi_{\mathrm{T},m})}, \qquad \in \mathbb{C}^{N_{\mathrm{R}}} \tag{1}$$

$$\mathbf{a}_{\mathrm{R},m}(\theta_{\mathrm{R},m}, \phi_{\mathrm{R},m}) \triangleq \frac{1}{\sqrt{N_{\mathrm{R}}}} e^{-j\boldsymbol{\Delta}_{\mathrm{R}}^{\mathrm{T}}\mathbf{k}(\theta_{\mathrm{R},m}, \phi_{\mathrm{R},m})}, \qquad \in \mathbb{C}^{N_{\mathrm{T}}} \tag{2}$$

where $\mathbf{k}(\theta, \phi) = \frac{2\pi}{\lambda}[\cos\phi \sin\theta, \sin\phi \sin\theta, \cos\theta]^{\mathrm{T}}$ is the wavenumber vector, λ is the wavelength, $\boldsymbol{\Delta}_{\mathrm{R}} \triangleq [\mathbf{u}_{\mathrm{R},1}, \mathbf{u}_{\mathrm{R},2}, \cdots, \mathbf{u}_{\mathrm{R},N_{\mathrm{R}}}]$, $\mathbf{u}_{\mathrm{R},n} \triangleq [x_{\mathrm{R},n}, y_{\mathrm{R},n}, z_{\mathrm{R},n}]^{\mathrm{T}}$ is a vector of Cartesian coordinates of the n^{th} receiver element, and N_{R} is the number of receiving antennas. N_{T}, $\boldsymbol{\Delta}_{\mathrm{T}}$ and $\mathbf{u}_{\mathrm{T},n}$ are defined similarly. We drop the angle parameters from the notation of $\mathbf{a}_{\mathrm{T},m},$ and $\mathbf{a}_{\mathrm{R},m}$.

[1]The subscripts T and R refer to the transmit and receive sides, respectively, regardless of using the uplink or downlink. On the other hand, when the notation is unique to the base station or the user equipment, we use the subscript BS and UE.

Denoting the TOA of the m^{th} path by τ_m, the channel can be expressed[2] as

$$\mathbf{H}(t) = \sum_{m=1}^{M} \mathbf{H}_m \delta(t - \tau_m), \tag{3}$$

From Fig. 1, $\tau_m = D_m/c$, where $D_m = d_{1,m} + d_{2,m}$, for $m > 1$ and

$$\mathbf{H}_m \triangleq \sqrt{N_{\text{R}} N_{\text{T}}} \beta_m \mathbf{a}_{\text{R},m} \mathbf{a}_{\text{T},m}^{\text{H}} \in \mathbb{C}^{N_{\text{R}} \times N_{\text{T}}}, \tag{4}$$

where β_m is the complex gain of the m^{th} path. Finally, we define the following vectors

$$\boldsymbol{\theta}_{\text{R}} \triangleq [\theta_{\text{R},1}, \theta_{\text{R},2}, ..., \theta_{\text{R},m}]^{\text{T}}, \qquad \boldsymbol{\theta}_{\text{T}} \triangleq [\theta_{\text{T},1}, \theta_{\text{T},2}, ..., \theta_{\text{T},m}]^{\text{T}}, \qquad \boldsymbol{\beta} \triangleq [\beta_1, \beta_2, ..., \beta_M]^{\text{T}},$$

$$\boldsymbol{\phi}_{\text{R}} \triangleq [\phi_{\text{R},1}, \phi_{\text{R},2}, ..., \phi_{\text{R},m}]^{\text{T}}, \qquad \boldsymbol{\phi}_{\text{T}} \triangleq [\phi_{\text{T},1}, \phi_{\text{T},2}, ..., \phi_{\text{T},m}]^{\text{T}}, \qquad \boldsymbol{\tau} \triangleq [\tau_1, \tau_2, ..., \tau_M]^{\text{T}}.$$

C. Transmission Model

The transmitter sends a signal $\sqrt{E_{\text{s}}}\mathbf{F}\mathbf{s}(t)$, where E_{s} is the transmitted energy per symbol duration, $\mathbf{F} \triangleq [\mathbf{f}_1, \mathbf{f}_2, ...\mathbf{f}_{N_{\text{B}}}]$ is a directional beamforming matrix, where

$$\mathbf{f}_\ell = \frac{1}{\sqrt{N_{\text{B}}}} \mathbf{a}_{\text{T},\ell}(\theta_\ell, \phi_\ell), \quad 1 \le \ell \le N_{\text{B}} \tag{5}$$

is a beam pointing towards (θ_ℓ, ϕ_ℓ) of the same form as (1), and N_{B} is the number of transmitted beams. The pilot signal $\mathbf{s}(t) \triangleq [s_1(t), s_2(t), ..., s_{N_{\text{B}}}(t)]^{\text{T}}$ is expressed as

$$s_\ell(t) = \sum_{k=0}^{N_{\text{s}}-1} a_{\ell,k} p(t - kT_{\text{s}}), \ 1 \le \ell \le N_{\text{B}}, \tag{6}$$

where $a_{\ell,k}$ are independent and identically distributed (IID) zero-mean unit-energy pilot symbols transmitted over the ℓ^{th} beam, and $p(t)$, is a unit-energy pulse with a power spectral density (PSD), denoted by $|P(f)|^2$. In (6), N_{s} is the number of pilot symbols and T_{s} is the symbol duration, leading to a total observation time of $T_{\text{o}} \approx N_{\text{s}} T_{\text{s}}$. To keep the transmitted power fixed with N_{T}, we set $\text{Tr}\left(\mathbf{F}^{\text{H}}\mathbf{F}\right) = 1$, $\mathbb{E}\{\mathbf{s}(t)\mathbf{s}^{\text{H}}(t)\} = \mathbf{I}_{N_{\text{B}}}$, where $\text{Tr}\,(\cdot)$ denotes the matrix trace, and $\mathbf{I}_{N_{\text{B}}}$ is the N_{B}-dimensional identity matrix.

The received signal observed at the input of the receive beamformer is given by

$$\mathbf{r}(t) \triangleq \sum_{m=1}^{M} \sqrt{E_{\text{s}}} \mathbf{H}_m \mathbf{F} \mathbf{s}(t - \tau_m) + \mathbf{n}(t), \quad t \in [0, T_{\text{o}}], \tag{7}$$

[2]We use a narrow-band array model, so that $A_{\text{max}} \ll c/W$, where A_{max} is maximum array aperture, c is speed of light, and W is the system bandwidth [24].

where $\mathbf{n}(t) \triangleq [n_1(t), n_2(t), ..., n_{N_\mathrm{T}}(t)]^\mathrm{T} \in \mathbb{C}^{N_\mathrm{R}}$ is zero-mean white Gaussian noise with PSD N_0. Similar to [25], [26], we assume that a low-noise amplifier and a passband filter are attached to each receive antenna. While this may seem a restrictive assumption, it will allow us to derive the PEB and OEB, which are fundamental lower bounds irrespective of the type of processing performed at the receiver, such as receive beamforming.

D. 3D Localization Problem

Our objective is to derive the UE PEB and OEB, based on the observed signal, $\mathbf{r}(t)$, for both the uplink and downlink. We achieve in two steps: firstly, we derive bounds on the channel parameters, namely, direction of arrival, $(\boldsymbol{\theta}_\mathrm{R}, \boldsymbol{\phi}_\mathrm{R})$, direction of departure, $(\boldsymbol{\theta}_\mathrm{T}, \boldsymbol{\phi}_\mathrm{T})$, time of arrival $\boldsymbol{\tau}$, and paths gains, $\boldsymbol{\beta}$. Secondly, we transform these bounds into the position domain.

III. Fisher Information Matrix of The Channel Parameters

We first derive exact expressions for the entries of the FIM. Then, we determine the conditions under which the individual paths can be considered orthogonal. Subsequently, we provide closed-form expressions of the CRLB for the single-path case for 3D and 2D localization.

A. Exact Expression

Let us define the parameter vector

$$\boldsymbol{\varphi} \triangleq [\boldsymbol{\theta}_\mathrm{R}^\mathrm{T}, \boldsymbol{\theta}_\mathrm{T}^\mathrm{T}, \boldsymbol{\phi}_\mathrm{R}^\mathrm{T}, \boldsymbol{\phi}_\mathrm{T}^\mathrm{T}, \boldsymbol{\tau}^\mathrm{T}, \boldsymbol{\beta}_\mathrm{R}^\mathrm{T}, \boldsymbol{\beta}_\mathrm{I}^\mathrm{T}]^\mathrm{T}, \tag{8}$$

where $\boldsymbol{\beta}_\mathrm{R} \triangleq \Re\{\boldsymbol{\beta}\}$, and $\boldsymbol{\beta}_\mathrm{I} \triangleq \Im\{\boldsymbol{\beta}\}$ are the real and imaginary parts of $\boldsymbol{\beta}$, respectively, and denote the u^{th} element in $\boldsymbol{\varphi}$ by φ_u, and the expectation with respect to the pilot symbols[3] by $\mathbb{E}_a[\cdot]$. Then, the corresponding FIM, partitioned into $M \times M$ submatrices, is structured as

$$\mathbf{J}_{\boldsymbol{\varphi}} \triangleq \begin{bmatrix} \mathbf{J}_{\boldsymbol{\theta}_\mathrm{R}\boldsymbol{\theta}_\mathrm{R}} & \mathbf{J}_{\boldsymbol{\theta}_\mathrm{R}\boldsymbol{\theta}_\mathrm{T}} & \cdots & \mathbf{J}_{\boldsymbol{\theta}_\mathrm{R}\boldsymbol{\beta}_\mathrm{I}} \\ \mathbf{J}_{\boldsymbol{\theta}_\mathrm{R}\boldsymbol{\theta}_\mathrm{T}}^\mathrm{T} & \ddots & \cdots & \vdots \\ \vdots & \cdots & \ddots & \vdots \\ \mathbf{J}_{\boldsymbol{\theta}_\mathrm{R}\boldsymbol{\tau}}^\mathrm{T} & \cdots & \cdots & \mathbf{J}_{\boldsymbol{\beta}_\mathrm{I}\boldsymbol{\beta}_\mathrm{I}} \end{bmatrix}, \tag{9}$$

[3]In fact, in this case the resulting bounds are called modified CRLB [27].

where, due to the additive white Gaussian noise [13],

$$[\mathbf{J}_{\boldsymbol{\varphi}}]_{u,v} \triangleq \frac{1}{N_0}\int_0^{T_{\rm o}} \mathbb{E}_a\left[\Re\left\{\frac{\partial \boldsymbol{\mu}_{\boldsymbol{\varphi}}^{\rm H}(t)}{\partial \varphi_u}\frac{\partial \boldsymbol{\mu}_{\boldsymbol{\varphi}}(t)}{\partial \varphi_v}\right\}\right]{\rm d}t, \tag{10}$$

$$\boldsymbol{\mu}_{\boldsymbol{\varphi}}(t) \triangleq \sqrt{N_{\rm R}N_{\rm T}E_{\rm s}}\sum_{m=1}^{M}\beta_m \mathbf{a}_{{\rm R},m}\mathbf{a}_{{\rm T},m}^{\rm H}\mathbf{F}\mathbf{s}(t-\tau_m). \tag{11}$$

We now introduce

$$\mathbf{B} \triangleq {\rm diag}(\boldsymbol{\beta}) \tag{12a}$$

$$\mathbf{A}_{\rm R} \triangleq [\mathbf{a}_{{\rm R},1}, \mathbf{a}_{{\rm R},2}, ..., \mathbf{a}_{{\rm R},N_{\rm R}}], \tag{12b}$$

$$\tilde{\mathbf{K}}_{{\rm R},m} \triangleq {\rm diag}\left(\frac{\partial}{\partial \theta_{{\rm R},m}}\boldsymbol{\Delta}_{\rm R}^{\rm T}\mathbf{k}(\theta_{{\rm R},m},\phi_{{\rm R},m})\right), \tag{12c}$$

$$\tilde{\mathbf{P}}_{{\rm R},m} \triangleq {\rm diag}\left(\frac{\partial}{\partial \phi_{{\rm R},m}}\boldsymbol{\Delta}_{\rm R}^{\rm T}\mathbf{k}(\theta_{{\rm R},m},\phi_{{\rm R},m})\right), \tag{12d}$$

$$\mathbf{K}_{\rm R} \triangleq [\tilde{\mathbf{K}}_{{\rm R},1}\mathbf{a}_{{\rm R},1}, \tilde{\mathbf{K}}_{{\rm R},2}\mathbf{a}_{{\rm R},2}, ..., \tilde{\mathbf{K}}_{{\rm R},N_{\rm R}}\mathbf{a}_{{\rm R},N_{\rm R}}], \tag{12e}$$

$$\mathbf{P}_{\rm R} \triangleq [\tilde{\mathbf{P}}_{{\rm R},1}\mathbf{a}_{{\rm R},1}, \tilde{\mathbf{P}}_{{\rm R},2}\mathbf{a}_{{\rm R},2}, ..., \tilde{\mathbf{P}}_{{\rm R},N_{\rm R}}\mathbf{a}_{{\rm R},N_{\rm R}}], \tag{12f}$$

with similar expression, obtained by replacing "R" with "T". It can be shown then that each submatrix in (9) is of the form

$$\mathbf{J}_{\mathbf{x},\mathbf{x}'} = \Re\left\{({\rm RX\ factor}) \odot ({\rm TX\ factor}) \odot ({\rm signal\ factor})\right\}, \tag{13}$$

where $\odot$ denotes the Hadamard product, the RX factor relates to the receiver array, the TX factor relates to the transmitter array and beamforming, and final factor relates to the pilot signal. The RX factor is a product of the matrices $\{\mathbf{A}_{\rm R}\mathbf{B}, \mathbf{K}_{\rm R}\mathbf{B}, \mathbf{P}_{\rm R}\mathbf{B}\}$, while the TX part is a product of similar matrices $\{\mathbf{F}^{\rm H}\mathbf{A}_{\rm T}, \mathbf{F}^{\rm H}\mathbf{K}_{\rm T}, \mathbf{F}^{\rm H}\mathbf{P}_{\rm T}\}$, associated with the transmitter as well as $\mathbf{F}$. Under the assumption of IID symbols, the signal factor depends on

$$[\mathbf{R}_i]_{uv} \triangleq \int_{-W/2}^{W/2}(2\pi f)^i |P(f)|^2 e^{-j2\pi f\Delta\tau_{uv}}{\rm d}f, \tag{14}$$

in which $\Delta\tau_{uv} \triangleq \tau_v - \tau_u$, $i \in \{0,1,2\}$, and W is the signal bandwidth. For instance, defining $\gamma \triangleq N_{\rm R}N_{\rm T}N_{\rm s}E_{\rm s}/N_0$, it can be verified that

$$\mathbf{J}_{\boldsymbol{\theta}_{\rm R}\boldsymbol{\theta}_{\rm R}} = \gamma\Re\left\{(\mathbf{B}^{\rm H}\mathbf{K}_{\rm R}^{\rm H}\mathbf{K}_{\rm R}\mathbf{B}) \odot (\mathbf{A}_{\rm T}^{\rm H}\mathbf{F}\mathbf{F}^{\rm H}\mathbf{A}_{\rm T})^{\rm T} \odot \mathbf{R}_0\right\}, \tag{15}$$

The rest of the FIM entries in (9) are listed in Appendix A, and all exhibit the structure in (13).

B. Approximate Fisher Information of the Channel Parameters

The exact FIMs presented in Section III-A provide the exact CRLB of the channel parameters. However, under some circumstances, it is possible to simplify this computation by reducing the submatrices of the FIMs to either diagonal or zero matrices, by exploiting the structure in (13). Inspired by [28], we start by introducing the following definition

Definition 1. *Given a diagonal matrix* $\mathbf{D}(\kappa) \neq \mathbf{0}$ *and a hollow matrix* $\mathbf{E}(\kappa) \neq \mathbf{0}$*, then a matrix* $\mathbf{A}(\kappa) = \mathbf{D}(\kappa) + \mathbf{E}(\kappa)$ *is almost diagonal (AD) for any parameter* κ *if*

$$\lim_{\kappa\to\infty} \delta(\mathbf{A}, \kappa) \triangleq \lim_{\kappa\to\infty} \frac{\|\mathbf{E}(\kappa)\|_{\mathrm{F}}}{\|\mathbf{D}(\kappa)\|_{\mathrm{F}}} = 0, \tag{16}$$

where $\|\cdot\|_{\mathrm{F}}$ *denotes the Frobenius norm.*

We now use this definition when inspecting the factors in (13), in order to understand the behavior under typical mmWave conditions, i.e., with large arrays at transmitter and receiver and large system bandwidth.

- *Factor 1 – Receiver Side:* For a large number of receive antennas, the power received from a direction $(\theta_{\mathrm{R},u}, \phi_{\mathrm{R},u})$ via a steering vector in the direction $(\theta_{\mathrm{R},v}, \phi_{\mathrm{R},v})$ is very small, i.e., $\|\mathbf{a}_{\mathrm{R},u}^{\mathrm{H}}\mathbf{a}_{\mathrm{R},v}\| \ll \|\mathbf{a}_{\mathrm{R},u}\|^2$, $u \neq v$, when the DOAs of the different paths are distinct. Thus, $\lim_{N_{\mathrm{R}}\to\infty} \delta(\mathbf{A}_{\mathrm{R}}^{\mathrm{H}}\mathbf{A}_{\mathrm{R}}, N_{\mathrm{R}}) = 0$. Similarly, considering the exponential form of $\mathbf{a}_{\mathrm{R},m}$ and that $\tilde{\mathbf{K}}_{\mathrm{R},m}, \tilde{\mathbf{P}}_{\mathrm{R},m}$ are diagonal,

  $$\lim_{N_{\mathrm{R}}\to\infty} \delta(\mathbf{K}_R^{\mathrm{H}}\mathbf{K}_{\mathrm{R}}, N_{\mathrm{R}}) = \lim_{N_{\mathrm{R}}\to\infty} \delta(\mathbf{P}_R^{\mathrm{H}}\mathbf{P}_{\mathrm{R}}, N_{\mathrm{R}}) = \lim_{N_{\mathrm{R}}\to\infty} \delta(\mathbf{K}_{\mathrm{R}}^{\mathrm{H}}\mathbf{P}_{\mathrm{R}}, N_{\mathrm{R}}) = 0.$$

  On the other hand, using the facts that the BS centroid is at the origin, then for uplink $\mathrm{Tr}(\tilde{\mathbf{K}}_{\mathrm{R},m}) = \mathrm{Tr}(\tilde{\mathbf{P}}_{\mathrm{R},m}) = 0$, and that the UE centroid is at $\mathbf{p}$, then for downlink $\mathrm{Tr}(\tilde{\mathbf{K}}_{\mathrm{R},m}) = \mathbf{p}^{\mathrm{T}}\frac{\partial}{\partial\theta_m}\mathbf{k}$, $\mathrm{Tr}(\tilde{\mathbf{P}}_{\mathrm{R},m}) = \mathbf{p}^{\mathrm{T}}\frac{\partial}{\partial\phi_m}\mathbf{k}$. Moreover, Noting that $[\mathbf{K}_{\mathrm{R}}^{\mathrm{H}}\mathbf{A}_{\mathrm{R}}]_{m,m} = \mathrm{Tr}(\tilde{\mathbf{K}}_{\mathrm{R},m})/N_{\mathrm{R}}$, then, for both uplink or downlink,

  $$\lim_{N_{\mathrm{R}}\to\infty} \mathbf{K}_{\mathrm{R}}^{\mathrm{H}}\mathbf{A}_{\mathrm{R}} = \lim_{N_{\mathrm{R}}\to\infty} \mathbf{P}_{\mathrm{R}}^{\mathrm{H}}\mathbf{A}_{\mathrm{R}} = \mathbf{0}_{M\times M}. \tag{18}$$

  where $\mathbf{0}_{M\times M}$ is an $M \times M$ matrix of zeros.
- *Factor 2 – Transmitter Side:* The transmitter side contributes to the FIM in (15) by $\mathbf{A}_{\mathrm{T}}^{\mathrm{H}}\mathbf{F}\mathbf{F}^{\mathrm{H}}\mathbf{A}_{\mathrm{T}}$ that can be shown to be AD matrix under certain conditions. Recalling that

  $$[\mathbf{A}_{\mathrm{T}}^{\mathrm{H}}\mathbf{F}\mathbf{F}^{\mathrm{H}}\mathbf{A}_{\mathrm{T}}]_{u,v} = \mathbf{a}_{\mathrm{T},u}^{\mathrm{H}}\mathbf{F}\mathbf{F}^{\mathrm{H}}\mathbf{a}_{\mathrm{T},v}, \tag{19}$$

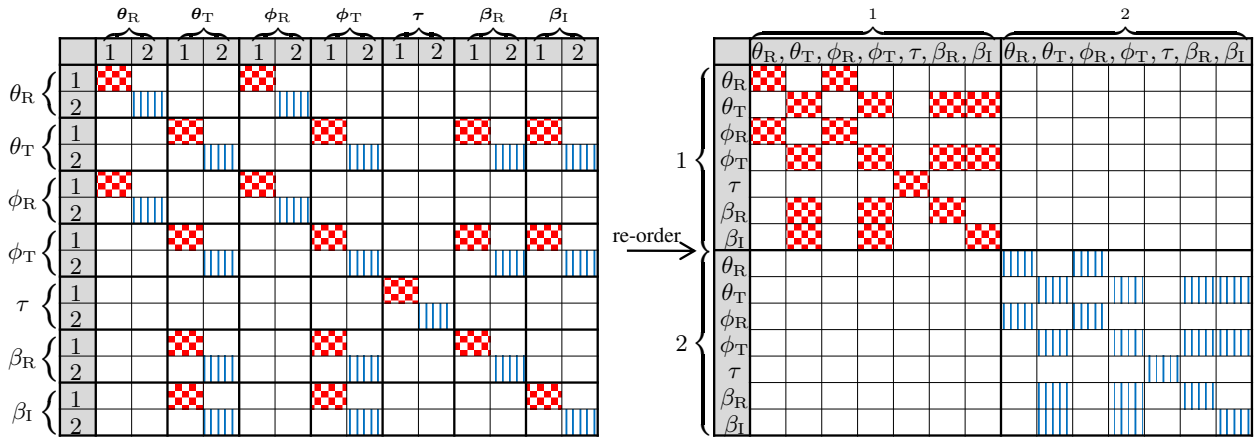

Fig. 2. An example on the approximate FIM in (9) with $M = 2$. The red-pattern and blue-strip cells represent the non-zero entries of the FIM and correspond to $m = 1$, and $m = 2$, respectively. Re-ordering the FIM on the left yields the FIMs in (37).

the right-hand side term can be interpreted as the spatial cross-correlation between the u^{th} and the v^{th} DODs caused by the beamforming. So, as N_{T} increases, the beams become narrower, and the spatial correlation vanishes,

$$\lim_{N_{\text{T}}\to\infty} \mathbf{a}_{\text{T},u}^{\text{H}} \mathbf{F}\mathbf{F}^{\text{H}} \mathbf{a}_{\text{T},v} = 0, \qquad \lim_{N_{\text{T}}\to\infty} \delta(\mathbf{A}_{\text{T}}^{\text{H}} \mathbf{F}\mathbf{F}^{\text{H}} \mathbf{A}_{\text{T}}, N_{\text{T}}) = 0. \tag{20}$$

Mathematically, (20) holds when $\mathbf{F}^{\text{H}}\mathbf{F}$ is AD itself, i.e., the beams are almost orthogonal. Thus, the strength of this factor requires high number of antennas and well-spaced beams. By inspection, a similar statement can be made for $(\mathbf{P}_{\text{T}}^{\text{H}} \mathbf{F}\mathbf{F}^{\text{H}} \mathbf{P}_{\text{T}})^{\text{T}}$, $(\mathbf{K}_{\text{T}}^{\text{H}} \mathbf{F}\mathbf{F}^{\text{H}} \mathbf{K}_{\text{T}})^{\text{T}}$, and $(\mathbf{P}_{\text{T}}^{\text{H}} \mathbf{F}\mathbf{F}^{\text{H}} \mathbf{K}_{\text{T}})^{\text{T}}$.

- *Factor 3: Multipath Cross-Correlation*: It can be shown that the cross-correlation functions in (14) are even for $i = 0, 2$ and have maxima on their diagonals. These maxima are constant with values 1 and $4\pi^2 W_{\text{eff}}^2$, respectively, where $W_{\text{eff}}^2 = \int_{-W/2}^{W/2} f^2 |P(f)|^2 \mathrm{d}f$. Moreover,

$$\lim_{W\to\infty} \delta(\mathbf{R}_0, W) = 0, \qquad \lim_{W\to\infty} \delta(\mathbf{R}_2, W) = 0. \tag{21}$$

Regarding $\mathbf{R}_1$, we note that for any W, $\mathrm{diag}(\mathbf{R}_1) = \mathbf{0}_{M\times M}$ so that $\mathbf{R}_1$ is a hollow matrix, with $\lim_{W\to\infty} \mathbf{R}_1 = \mathbf{0}_{M\times M}$.

In combination, given the Hadamard product structure of (13), we find that under typical mmWave conditions, due to the combined effect of large values of $N_{\text{R}}, N_{\text{T}}, W$, some submatrices of the FIM in (9) are AD, while the others are almost zero. This effect relates to the fact that paths can be resolved in either direction of arrival, direction or departure, or delay domain, all of which enforce each other in mmWave. This effect is visualized in Fig. 2 (left). Re-ordering the parameters, grouping them path by path, we obtain the block diagonal FIM in Fig. 2 (right).

C. FIM of Single-Path mmWave Channel Parameters

In this section, we use the notion of the equivalent FIM (EFIM) from [18]. EFIM is a measure of the information corresponding to a certain unknown parameter, taking into account the uncertainties of the other unknown parameters.

Definition 2. *Given a parameter vector* $\boldsymbol{\theta} \triangleq [\boldsymbol{\theta}_1^{\mathrm{T}}, \boldsymbol{\theta}_2^{\mathrm{T}}]^{\mathrm{T}}$ *with corresponding FIM*

$$\mathbf{J}_{\boldsymbol{\theta}\boldsymbol{\theta}} = \begin{bmatrix} \mathbf{J}_{\boldsymbol{\theta}_1\boldsymbol{\theta}_1} & \mathbf{J}_{\boldsymbol{\theta}_1\boldsymbol{\theta}_2} \\ \mathbf{J}_{\boldsymbol{\theta}_1\boldsymbol{\theta}_2}^{\mathrm{T}} & \mathbf{J}_{\boldsymbol{\theta}_2\boldsymbol{\theta}_2} \end{bmatrix}, \tag{22}$$

Then, the EFIM of $\boldsymbol{\theta}_1$ *is given by*

$$\mathbf{J}^{\mathrm{e}}_{\boldsymbol{\theta}_1\boldsymbol{\theta}_1} = \mathbf{J}_{\boldsymbol{\theta}_1\boldsymbol{\theta}_1} - \mathbf{J}_{\boldsymbol{\theta}_1\boldsymbol{\theta}_2}\mathbf{J}^{-1}_{\boldsymbol{\theta}_2\boldsymbol{\theta}_2}\mathbf{J}^{\mathrm{T}}_{\boldsymbol{\theta}_1\boldsymbol{\theta}_2}. \tag{23}$$

Given the block-diagonal structure of the approximate FIM, it becomes meaningful to study paths separately. Thus, dropping the path index m and considering β as a nuisance parameter, we focus on a single path, with the parameters of interest being $\boldsymbol{\varphi}_{\mathrm{ch}} \triangleq [\theta_{\mathrm{R}}, \theta_{\mathrm{T}}, \phi_{\mathrm{R}}, \phi_{\mathrm{T}}, \tau]^{\mathrm{T}}$, and write the EFIM of the DOA, DOD, and TOA, from Appendix B, as follows

$$\mathbf{J}^{\mathrm{e}}_{\boldsymbol{\varphi}_{\mathrm{ch}}} = \gamma|\beta|^2 \begin{bmatrix} \mathbf{J}^{\mathrm{e}}_{\boldsymbol{\theta},\boldsymbol{\phi}} & \mathbf{0}_4 \\ \mathbf{0}_4^{\mathrm{T}} & 4\pi^2 G W^2_{\mathrm{eff}} \end{bmatrix}, \tag{24}$$

where

$$\mathbf{J}^{\mathrm{e}}_{\boldsymbol{\theta},\boldsymbol{\phi}} = \gamma|\beta|^2 \begin{bmatrix} R_\theta G & 0 & X_{\theta,\phi} G & 0 \\ 0 & \frac{L_\theta}{G} & 0 & \frac{Y_{\theta,\phi}}{G} \\ X_{\theta,\phi} G & 0 & R_\phi G & 0 \\ 0 & \frac{Y_{\theta,\phi}}{G} & 0 & \frac{L_\phi}{G} \end{bmatrix}, \tag{25}$$

in which

$$\begin{aligned} &R_\theta \triangleq \mathbf{a}_{\mathrm{R}}^{\mathrm{H}} \mathbf{K}_{\mathrm{R}}^2 \mathbf{a}_{\mathrm{R}}, && L_\theta \triangleq G T_\theta - |V_\theta|^2, && G \triangleq \mathbf{a}_{\mathrm{T}}^{\mathrm{H}} \mathbf{F}\mathbf{F}^{\mathrm{H}} \mathbf{a}_{\mathrm{T}}, \\ &R_\phi \triangleq \mathbf{a}_{\mathrm{R}}^{\mathrm{H}} \mathbf{P}_{\mathrm{R}}^2 \mathbf{a}_{\mathrm{R}}, && L_\phi \triangleq G T_\phi - |V_\phi|^2, && X_{\theta,\phi} \triangleq \mathbf{a}_{\mathrm{R}}^{\mathrm{H}} \mathbf{K}_{\mathrm{R}} \mathbf{P}_{\mathrm{R}} \mathbf{a}_{\mathrm{R}}, \\ &V_\theta \triangleq \mathbf{a}_{\mathrm{T}}^{\mathrm{H}} \mathbf{K}_{\mathrm{T}} \mathbf{F}\mathbf{F}^{\mathrm{H}} \mathbf{a}_{\mathrm{T}}, && T_\theta \triangleq \mathbf{a}_{\mathrm{T}}^{\mathrm{H}} \mathbf{K}_{\mathrm{T}} \mathbf{F}\mathbf{F}^{\mathrm{H}} \mathbf{K}_{\mathrm{T}} \mathbf{a}_{\mathrm{T}}, && Y_{\theta,\phi} \triangleq G Y'_{\theta,\phi} - \Re\{V_\phi V_\theta^*\}, \\ &V_\phi \triangleq \mathbf{a}_{\mathrm{T}}^{\mathrm{H}} \mathbf{P}_{\mathrm{T}} \mathbf{F}\mathbf{F}^{\mathrm{H}} \mathbf{a}_{\mathrm{T}}. && T_\phi \triangleq \mathbf{a}_{\mathrm{T}}^{\mathrm{H}} \mathbf{P}_{\mathrm{T}} \mathbf{F}\mathbf{F}^{\mathrm{H}} \mathbf{P}_{\mathrm{T}} \mathbf{a}_{\mathrm{T}}, && Y'_{\theta,\phi} \triangleq \Re\{\mathbf{a}_{\mathrm{T}}^{\mathrm{H}} \mathbf{P}_{\mathrm{T}} \mathbf{F}\mathbf{F}^{\mathrm{H}} \mathbf{K}_{\mathrm{T}} \mathbf{a}_{\mathrm{T}}\}, \end{aligned}$$

The following proposition, highlights how to compute the CRLB of the channel parameters for arbitrary array geometries.

Proposition 1. *Based on the FIM in (24), the CRLBs of the DOA, DOD and TOA are given by*

$$\mathrm{CRLB}\left(\theta_{\mathrm{R}}\right) = \frac{R_\phi}{\gamma\zeta_1|\beta|^2 G}, \tag{26a}$$

$$\mathrm{CRLB}\left(\phi_{\mathrm{R}}\right) = \frac{R_\theta}{\gamma\zeta_1|\beta|^2 G}, \tag{26b}$$

$$\mathrm{CRLB}\left(\theta_{\mathrm{T}}\right) = \frac{GL_\phi}{\gamma\zeta_2|\beta|^2}, \tag{26c}$$

$$\mathrm{CRLB}\left(\phi_{\mathrm{T}}\right) = \frac{GL_\theta}{\gamma\zeta_2|\beta|^2}, \tag{26d}$$

$$\mathrm{CRLB}(\tau) = \frac{1}{4\gamma\pi^2 W_{\mathrm{eff}}^2|\beta|^2 G}. \tag{26e}$$

where $\zeta_1 = R_\theta R_\phi - X_{\theta,\phi}^2$, *and* $\zeta_2 = L_\theta L_\phi - Y_{\theta,\phi}^2$.

Proof. See Appendix B. □

Note that for 2D localization, when the UE and BS are located in the xy-plane, $\theta_{\mathrm{R}} = \theta_{\mathrm{T}} = \pi/2$ are known so they can be removed from $\boldsymbol{\varphi}_{ch}$, leading to

$$\mathrm{CRLB}(\phi_{\mathrm{R}}) = \frac{1}{\gamma|\beta|^2 R_\phi G}, \tag{27a}$$

$$\mathrm{CRLB}(\phi_{\mathrm{T}}) = \frac{G}{\gamma|\beta|^2 L_\phi}, \tag{27b}$$

while $\mathrm{CRLB}(\tau)$ is unchanged. Appendix C provides details on how the FIM and CRLB can be computed for the special cases of URA and ULA.

IV. Fisher Information of the Location Parameters

In the preceding sections, we have seen how the FIM of the multipath channel parameters can be approximated by multiple single-path FIMs. We have also derived the single-path FIM for different settings. In this section, we derive the PEB and the OEB by applying a transformation [13] to the EFIM of DOA, DOD, and TOA, computed from (9), to obtain the exact FIM of position and orientation. We also transform $\mathbf{J}_{\boldsymbol{\varphi}_{\mathrm{ch}}}$, defined in (24), to obtain the approximate one.

A. PEB and OEB: Exact Approach

1) General Formulation: In this section, we derive the PEB and OEB based on the EFIM of the multipath channel parameters of interest $\boldsymbol{\varphi}_{\mathrm{CH}} \triangleq [\boldsymbol{\theta}^{\mathrm{T}}, \boldsymbol{\phi}^{\mathrm{T}}, \boldsymbol{\tau}^{\mathrm{T}}]^{\mathrm{T}}$. We do so by first transforming $\mathbf{J}^{\mathrm{e}}_{\boldsymbol{\varphi}_{\mathrm{CH}}}$ to a FIM of the location parameters $\boldsymbol{\varphi}_{\mathrm{L}} \triangleq [\mathbf{o}^{\mathrm{T}}, \mathbf{p}^{\mathrm{T}}, \mathbf{q}^{\mathrm{T}}]^{\mathrm{T}}$, where

$$\boldsymbol{\theta} = \left[\boldsymbol{\theta}_{\mathrm{R}}^{\mathrm{T}}, \boldsymbol{\theta}_{\mathrm{T}}^{\mathrm{T}}\right]^{\mathrm{T}}, \qquad \boldsymbol{\phi} = \left[\boldsymbol{\phi}_{\mathrm{R}}^{\mathrm{T}}, \boldsymbol{\phi}_{\mathrm{T}}^{\mathrm{T}}\right]^{\mathrm{T}}, \qquad \mathbf{q} \triangleq \left[\mathbf{q}_2^{\mathrm{T}}, \mathbf{q}_3^{\mathrm{T}}, \cdots, \mathbf{q}_M^{\mathrm{T}}\right]^{\mathrm{T}}.$$

Towards that, we write

$$\mathbf{J}_{\boldsymbol{\varphi}_{\mathrm{L}}} \triangleq \boldsymbol{\Upsilon}\mathbf{J}^{\mathrm{e}}_{\boldsymbol{\varphi}_{\mathrm{CH}}}\boldsymbol{\Upsilon}^{\mathrm{T}} \triangleq \begin{bmatrix} \boldsymbol{\Psi} & \boldsymbol{\Phi} \\ \boldsymbol{\Phi}^{\mathrm{T}} & \boldsymbol{\Omega} \end{bmatrix}, \tag{28}$$

where $\boldsymbol{\Psi} \in \mathbb{R}^{5\times 5}$, $\boldsymbol{\Omega} \in \mathbb{R}^{3(M-1)\times 3(M-1)}$ and

$$\boldsymbol{\Upsilon} \triangleq \begin{bmatrix} \frac{\partial \boldsymbol{\theta}^{\mathrm{T}}}{\partial \mathbf{o}} & \frac{\partial \boldsymbol{\phi}^{\mathrm{T}}}{\partial \mathbf{o}} & \frac{\partial \boldsymbol{\tau}^{\mathrm{T}}}{\partial \mathbf{o}} \\ \frac{\partial \boldsymbol{\theta}^{\mathrm{T}}}{\partial \mathbf{p}} & \frac{\partial \boldsymbol{\phi}^{\mathrm{T}}}{\partial \mathbf{p}} & \frac{\partial \boldsymbol{\tau}^{\mathrm{T}}}{\partial \mathbf{p}} \\ \frac{\partial \boldsymbol{\theta}^{\mathrm{T}}}{\partial \mathbf{q}} & \frac{\partial \boldsymbol{\phi}^{\mathrm{T}}}{\partial \mathbf{q}} & \frac{\partial \boldsymbol{\tau}^{\mathrm{T}}}{\partial \mathbf{q}} \end{bmatrix}. \tag{29}$$

Consequently, the EFIM of the position $\mathbf{p}$ and orientation $\mathbf{o}$ is found via Schur's complement as

$$\mathbf{J}^{\mathrm{e}}_{\mathbf{o},\mathbf{p}} = \boldsymbol{\Psi} - \boldsymbol{\Phi}\boldsymbol{\Omega}^{-1}\boldsymbol{\Phi}^{\mathrm{T}}. \tag{30}$$

Finally, the PEB and OEB are given by the square roots of the squared-PEB (SPEB) and squared-OEB (SOEB) defined as

$$\mathrm{SOEB} = \left[(\mathbf{J}^{\mathrm{e}}_{\mathbf{o},\mathbf{p}})^{-1}\right]_{1,1} + \left[(\mathbf{J}^{\mathrm{e}}_{\mathbf{o},\mathbf{p}})^{-1}\right]_{2,2}, \tag{31a}$$

$$\mathrm{SPEB} = \left[(\mathbf{J}^{\mathrm{e}}_{\mathbf{o},\mathbf{p}})^{-1}\right]_{3,3} + \left[(\mathbf{J}^{\mathrm{e}}_{\mathbf{o},\mathbf{p}})^{-1}\right]_{4,4} + \left[(\mathbf{J}^{\mathrm{e}}_{\mathbf{o},\mathbf{p}})^{-1}\right]_{5,5}. \tag{31b}$$

2) Transformation for Uplink and Downlink: The relationships governing the UE position and orientation with the BS and UE angles are different. Therefore, unlike $\mathbf{J}_{\boldsymbol{\varphi}}$, the structure of $\boldsymbol{\Upsilon}$ and, effectively, $\mathbf{J}^{\mathrm{e}}_{\mathbf{o},\mathbf{p}}$, depends on whether the uplink or downlink is used for signal transmission. For this reason, we switch to the explicit notation with the subscripts BS and UE,

$$\boldsymbol{\theta} = \begin{cases} \left[\boldsymbol{\theta}^{\mathrm{T}}_{\mathrm{BS}}, \boldsymbol{\theta}^{\mathrm{T}}_{\mathrm{UE}}\right]^{\mathrm{T}}, & \text{uplink} \\ \left[\boldsymbol{\theta}^{\mathrm{T}}_{\mathrm{UE}}, \boldsymbol{\theta}^{\mathrm{T}}_{\mathrm{BS}}\right]^{\mathrm{T}}, & \text{downlink} \end{cases}, \qquad \boldsymbol{\phi} = \begin{cases} \left[\boldsymbol{\phi}^{\mathrm{T}}_{\mathrm{BS}}, \boldsymbol{\phi}^{\mathrm{T}}_{\mathrm{UE}}\right]^{\mathrm{T}}, & \text{uplink} \\ \left[\boldsymbol{\phi}^{\mathrm{T}}_{\mathrm{UE}}, \boldsymbol{\phi}^{\mathrm{T}}_{\mathrm{BS}}\right]^{\mathrm{T}}, & \text{downlink}. \end{cases} \tag{32}$$

where $\boldsymbol{\theta}_{\mathrm{BS}}$ and $\boldsymbol{\phi}_{\mathrm{BS}}$ denote the vectors of the angles at the BS, and $\boldsymbol{\theta}_{\mathrm{UE}}$ and $\boldsymbol{\phi}_{\mathrm{UE}}$ at the UE.

With the BS located at the origin, the geometry relating the LOS angle parameters is illustrated in Fig. 3. From this figure, we can derive the following equations

$$\theta_{\mathrm{UE},1} = \theta_0 - \tan^{-1}\left(p_y/p_z\right) + \pi, \tag{33a}$$

$$\phi_{\mathrm{UE},1} = -\phi_0 + \tan^{-1}\left(p_y/p_x\right) + \pi, \tag{33b}$$

$$\theta_{\mathrm{BS},1} = \tan^{-1}\left(p_y/p_z\right), \tag{33c}$$

$$\phi_{\mathrm{BS},1} = \tan^{-1}\left(p_y/p_x\right), \tag{33d}$$

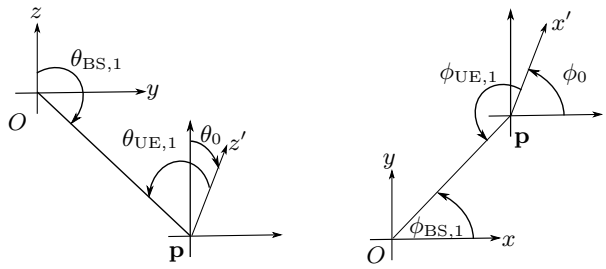

Fig. 3. LOS relationship between orientation angles and the angles of BS and UE, in the Elevation (left), and Azimuth (right).

$$\tau_1 = \|\mathbf{p}\|/c. \tag{33e}$$

Now, it is straight-forward to see that the corresponding elements in the transformation defined in (29) can be obtained as follows

$$\frac{\partial \theta_{\mathrm{UE},1}}{\partial \theta_0} = -\frac{\partial \phi_{\mathrm{UE},1}}{\partial \phi_0} = 1, \tag{34a}$$

$$\frac{\partial \theta_{\mathrm{BS},1}}{\partial \mathbf{p}} = -\frac{\partial \theta_{\mathrm{UE},1}}{\partial \mathbf{p}} = \frac{[0, p_z, -p_y]^{\mathrm{T}}}{p_y^2 + p_z^2}, \tag{34b}$$

$$\frac{\partial \phi_{\mathrm{BS},1}}{\partial \mathbf{p}} = \frac{\partial \phi_{\mathrm{UE},1}}{\partial \mathbf{p}} = \frac{[-p_y, p_x, 0]^{\mathrm{T}}}{p_x^2 + p_y^2}, \tag{34c}$$

$$\frac{\partial \tau_1}{\partial \mathbf{p}} = \frac{\mathbf{p}}{c\|\mathbf{p}\|}. \tag{34d}$$

Note that derivatives of the BS angles w.r.t. orientation angles are zero. This is a distinctive difference between the uplink and downlink. For NLOS paths, the geometrical relationships of the angle parameters of the m^{th} path are shown in Fig. 4. These relationships can be written as

$$\theta_{\mathrm{UE},m} = \theta_0 + \tan^{-1}\left(w_{m,y}/w_{m,z}\right), \tag{35a}$$

$$\phi_{\mathrm{UE},m} = -\phi_0 + \tan^{-1}\left(w_{m,y}/w_{m,x}\right), \tag{35b}$$

$$\theta_{\mathrm{BS},m} = \tan^{-1}\left(q_{m,y}/q_{m,z}\right), \tag{35c}$$

$$\phi_{\mathrm{BS},m} = \tan^{-1}\left(q_{m,y}/q_{m,x}\right), \tag{35d}$$

$$\tau_m = \left(\|\mathbf{q}_m\| + \|\mathbf{w}_m\|\right)/c. \tag{35e}$$

where $\mathbf{w}_m \triangleq [w_{m,x}, w_{m,y}, w_{m,z}]^{\mathrm{T}} = \mathbf{q}_m - \mathbf{p}$. As a result,

$$\frac{\partial \theta_{\mathrm{UE},m}}{\partial \theta_0} = -\frac{\partial \phi_{\mathrm{UE},m}}{\partial \phi_0} = 1, \tag{36a}$$

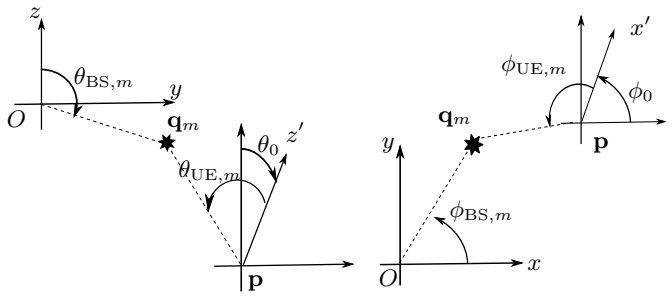

Fig. 4. NLOS relationship between orientation angles and the angles of BS and UE, in the Elevation (left), and Azimuth (right).

$$\frac{\partial \theta_{\mathrm{UE},m}}{\partial \mathbf{p}} = -\frac{\partial \theta_{\mathrm{UE},m}}{\partial \mathbf{q}_m} = \frac{[0, -w_{m,z}, w_{m,y}]^{\mathrm{T}}}{w_{m,y}^2 + w_{m,z}^2}, \tag{36b}$$

$$\frac{\partial \phi_{\mathrm{UE},m}}{\partial \mathbf{p}} = -\frac{\partial \phi_{\mathrm{UE},m}}{\partial \mathbf{q}_m} = \frac{[w_{m,y}, -w_{m,x}, 0]^{\mathrm{T}}}{w_{m,x}^2 + w_{m,y}^2}, \tag{36c}$$

$$\frac{\partial \tau_m}{\partial \mathbf{p}} = -\frac{\mathbf{w}_m}{c\|\mathbf{w}_m\|}, \tag{36d}$$

$$\frac{\partial \theta_{\mathrm{BS},m}}{\partial \mathbf{q}_m} = \frac{[0, q_{m,z}, -q_{m,y}]^{\mathrm{T}}}{q_{m,y}^2 + q_{m,z}^2}, \tag{36e}$$

$$\frac{\partial \phi_{\mathrm{BS},m}}{\partial \mathbf{q}_m} = \frac{[-q_{m,y}, q_{m,x}, 0]^{\mathrm{T}}}{q_{m,x}^2 + q_{m,y}^2}, \tag{36f}$$

$$\frac{\partial \tau_m}{\partial \mathbf{q}_m} = \frac{1}{c}\left(\frac{\mathbf{q}_m}{\|\mathbf{q}_m\|} + \frac{\mathbf{w}_m}{\|\mathbf{w}_m\|}\right). \tag{36g}$$

Substitution into $\boldsymbol{\Upsilon}$ yields the FIM of the location parameters.

B. PEB and OEB: Approximate Approach

In Section III-B, it was concluded that, under certain conditions, the multiple paths arriving at the receiver can be treated as non-interfering paths carrying independent information. Thus, we can write the total FIM of position and orientation as a sum of the individual FIMs obtained by transforming the CRLBs of DODs, DOAs, and TOAs of these paths individually.

Proposition 2. *Let* $\mathbf{J}_{\boldsymbol{\varphi}_s}^{(m)}$ *be the FIM of the* m^{th} *path parameters depicted in Fig. 2 (left), so that*

$$\mathbf{J}_{\boldsymbol{\varphi}_s}^{(m)} \triangleq \begin{bmatrix} \boldsymbol{\Lambda}_m & \boldsymbol{\Pi}_m \\ \boldsymbol{\Pi}_m^{\mathrm{T}} & \boldsymbol{\Xi}_m \end{bmatrix}, \tag{37}$$

where $\boldsymbol{\Lambda}_m$ *is the* 5×5 *FIM of* $\theta_{\mathrm{R},m}, \theta_{\mathrm{T},m}, \phi_{\mathrm{R},m}, \phi_{\mathrm{T},m}$, *and* τ_m, *and* $\boldsymbol{\Xi}_m$ *is the* 2×2 *FIM of* $\beta_{\mathrm{R},m}$

and $\beta_{\mathrm{I},m}$. Moreover, denote the EFIM of the m^{th} DOA, DOD, and TOA by

$$\mathbf{\Lambda}_m^{\mathrm{e}} = \mathbf{\Lambda}_m - \mathbf{\Pi}_m \mathbf{\Xi}_m^{-1} \mathbf{\Pi}_m^{\mathrm{T}}, \tag{38}$$

and the corresponding transformation matrix in block form by

$$\mathbf{\Upsilon}_m \triangleq \begin{cases} \overline{\mathbf{\Upsilon}}_1, & m = 1 \\ \begin{bmatrix} \overline{\mathbf{\Upsilon}}_m^{\mathrm{T}} & \overline{\overline{\mathbf{\Upsilon}}}_m^{\mathrm{T}} \end{bmatrix}^{\mathrm{T}}, & 2 \leq m \leq M \end{cases} \tag{39}$$

where $\overline{\mathbf{\Upsilon}}_m$ is the 5×5 matrix relating to $\mathbf{o}$ and $\mathbf{p}$, and $\overline{\overline{\mathbf{\Upsilon}}}_m$ is the 3×5 matrix relating to $\mathbf{q}_m$. Then, the approximate EFIM of $\mathbf{o}$ and $\mathbf{p}$ is given by

$$\begin{aligned} \tilde{\mathbf{J}}_{\mathbf{o},\mathbf{p}}^{\mathrm{e}} \triangleq \sum_{m=1}^{M} \mathbf{J}_{\mathbf{o},\mathbf{p}}^{(m)} &= \sum_{m=1}^{M} \overline{\mathbf{\Upsilon}}_m \mathbf{\Lambda}_m \overline{\mathbf{\Upsilon}}_m^{\mathrm{T}} \\ &\quad - \underbrace{\sum_{m=1}^{M} \overline{\mathbf{\Upsilon}}_m \mathbf{\Pi}_m \mathbf{\Xi}_m^{-1} \mathbf{\Pi}_m^{\mathrm{T}} \overline{\mathbf{\Upsilon}}_m^{\mathrm{T}}}_{\text{path gains uncertainty}} - \underbrace{\sum_{m=2}^{M} \overline{\mathbf{\Upsilon}}_m \mathbf{\Lambda}_m^{\mathrm{e}} \overline{\overline{\mathbf{\Upsilon}}}_m^{\mathrm{T}} \left(\overline{\overline{\mathbf{\Upsilon}}} \mathbf{\Lambda}_m^{\mathrm{e}} \overline{\overline{\mathbf{\Upsilon}}}^{\mathrm{T}} \right)^{-1} \overline{\overline{\mathbf{\Upsilon}}}_m \mathbf{\Lambda}_m^{\mathrm{e}} \overline{\mathbf{\Upsilon}}_m^{\mathrm{T}}}_{\text{clusters locations uncertainty}}. \end{aligned} \tag{40}$$

Proof. See Appendix D. □

Note that $\mathbf{\Lambda}_m^{\mathrm{e}}$ equals (24) evaluated for the m^{th} path.

C. Closed-Form Expressions for LOS: 3D and 2D

Although it is hard to derive closed-form solution of the general case of PEB and OEB, here we present expressions for the LOS case. First, we introduce the following notation

$$\tilde{\zeta_1} \triangleq \frac{A_2}{\sin^2 \phi_{\mathrm{BS}}} \left(A_1 R_\theta + A_2 R_\phi + A_3 X_{\theta,\phi} \right) \tag{41a}$$

$$\tilde{\zeta_2} \triangleq \frac{A_2}{\sin^2 \phi_{\mathrm{BS}}} \left(A_1 L_\theta + A_2 L_\phi + A_3 Y_{\theta,\phi} \right), \tag{41b}$$

where $A_1 \triangleq \sin^2 \theta_{\mathrm{BS}}$, $A_2 \triangleq \cos^2 \theta_{\mathrm{BS}} + \sin^2 \theta_{\mathrm{BS}} \sin^2 \phi_{\mathrm{BS}}$, and $A_3 \triangleq 2 \cos \theta_{\mathrm{BS}} \cos \phi_{\mathrm{BS}} \sin \theta_{\mathrm{BS}}$.

Proposition 3. *For the localization problem set in Section II, in the existence of a LOS path only, the 3D localization PEB and OEB of a UE located at $\mathbf{p}$ with an orientation angle $\mathbf{o}$ are given by*

$$\mathrm{SOEB} = \frac{G \left(L_\theta + L_\phi \right)}{\gamma \zeta_2 |\beta|^2} + \frac{\left(R_\theta + R_\phi \right)}{\zeta_1 \gamma |\beta|^2 G}. \tag{42a}$$

TABLE I
SCALING FACTORS OF CRLBS OF THE CHANNEL PARAMETERS, PEB AND OEB

	$\mathrm{CRB}(\theta_{\mathrm{R}})$	$\mathrm{CRB}(\theta_{\mathrm{T}})$	$\mathrm{CRB}(\phi_{\mathrm{R}})$	$\mathrm{CRB}(\phi_{\mathrm{T}})$	$\mathrm{CRB}(\tau)$	SOEB	SPEB (DL)	SPEB (UL)
URA	N_{R}^{-2}	N_{R}^{-1}	N_{R}^{-2}	N_{R}^{-1}	N_{R}^{-1}	$N_{\mathrm{R}}^{-1}+N_{\mathrm{R}}^{-2}$	N_{R}^{-1}	$N_{\mathrm{R}}^{-1}+N_{\mathrm{R}}^{-2}$
ULA	N/A	N/A	N_{R}^{-3}	N_{R}^{-1}	N_{R}^{-1}	$N_{\mathrm{R}}^{-1}+N_{\mathrm{R}}^{-3}$	N_{R}^{-1}	$N_{\mathrm{R}}^{-1}+N_{\mathrm{R}}^{-3}$

$$\mathrm{SPEB}=\frac{c^2}{4\gamma\pi^2|\beta|^2GW_{\mathrm{eff}}^2}+\frac{\|\mathbf{p}\|^2}{|\beta|^2\gamma}\times\begin{cases}\tilde{\zeta}_1/(\zeta_1 G) & \text{uplink}\\ \tilde{\zeta}_2 G/\zeta_2 & \text{downlink}\end{cases}. \tag{42b}$$

where ζ_1,ζ_2 are as defined in Proposition 1. For the 2D localization

$$\mathrm{SOEB}=\frac{1}{\gamma|\beta|^2GR_\phi}+\frac{G}{\gamma|\beta|^2L_\phi}, \tag{43a}$$

$$\mathrm{SPEB}=\frac{c^2}{4\gamma\pi^2|\beta|^2GW_{\mathrm{eff}}^2}+\frac{\|\mathbf{p}\|^2}{|\beta|^2\gamma}\times\begin{cases}1/(R_\phi G) & \text{uplink}\\ G/L_\phi & \text{downlink}\end{cases}. \tag{43b}$$

Proof. See Appendix E. □

Note that, since $\zeta_1,\tilde{\zeta}_1$ depend on the DOA, and that $\zeta_2,\tilde{\zeta}_2$ depend on the DOED, it is straightforward to see that the PEB is a function of the TOA and either DOA (in uplink) or DOD (in downlink). Since the CRLBs of DOD and DOA are not identical in (26), the PEB depends on whether communication is in uplink or downlink. On the other hand, the orientation depends on both the DOA and DOD in a symmetric relationship (see (33)). Hence, the OEB is the same for uplink and downlink. Finally, observe that due to (26)–(27), in the 2D case $\mathrm{SOEB}=\mathrm{CRLB}(\phi_{\mathrm{R}})+\mathrm{CRLB}(\phi_{\mathrm{T}})$ and $\mathrm{SPEB}=c^2\,\mathrm{CRLB}(\tau)+\|\mathbf{p}\|^2\,\mathrm{CRLB}(\phi_{\mathrm{BS}})$.

These results can be used to determine scaling laws. For instance, evaluating (26) and (42) as a function of N_{R}, the scaling factors in Table I are obtained. Similarly the scaling factors for ULA are obtained in [29]. We see that URAs and ULAs have different scaling, in that for $\mathrm{CRLB}(\phi_{\mathrm{R}})$ scales with $1/N_{\mathrm{R}}^2$ for URAs, but with $1/N_{\mathrm{R}}^3$ for ULAs. This can be explained by noting that these scaling factor consist of two multiplicative components: SNR imporvement that scales with $1/N_{\mathrm{R}}$ for both geometries, and a spatial resolution that depends on the squared number of antennas in the direction of x-axis, that is $1/N_{\mathrm{R}}^2$ for ULAs, and $1/(\sqrt{N_{\mathrm{R}}})^2$ for URAs.

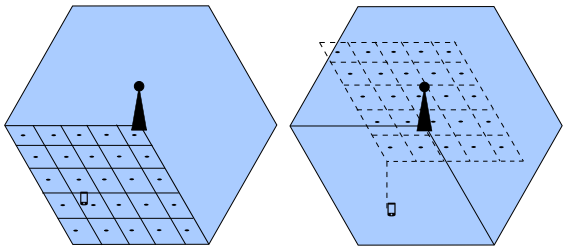

Fig. 5. A cell sectorized into three sectors, each served by 25 beams directed towards a grid on the ground in the downlink (left) and towards a virtual grid in uplink (right). The grid has the same orientation as the UE.

V. Numerical Results and Discussion

A. Simulation Environment

Although the theoretical results are valid for any arbitrary array geometry, we focus on URAs, as an example of 3D localization. Particularly, we consider a scenario where a BS with square array is located in the xz-plane centered at the origin with $\sqrt{N_{\rm BS}} \times \sqrt{N_{\rm BS}}$ antenna elements and a height of 10 meters. The UE, operating at $f = 38$ GHz, is equipped with a square array which have $\sqrt{N_{\rm UE}} \times \sqrt{N_{\rm UE}}$ antenna elements, and assumed to be tilted with some orientation angle. We investigate the performance over a flat 120° sector of a sectorized cell with a radius of 50 meters. The UE is assumed to be located anywhere in this sector. Moreover, we consider an ideal sinc pulse so that $W_{\rm eff}^2 = W^2/12$, where $W = 125$ MHz, $E_{\rm s}T_{\rm s} = 0$ dBm, $N_0 = -170$ dBm/Hz, and $N_{\rm s} = 16$ pilot symbols. We utilize the directional beamforming scheme defined in (5). In the downlink case, the directions of the beams are chosen such that the beams centers are equispaced on the ground. On the other hand, in the uplink, the UE transmits beams equispaced on a virtual sector in the horizontal plane containing the BS. Fig. 5 depicts an example with $N_{\rm B} = 25$ for both uplink and downlink. The environment comprises scatterers and reflectors, with scatterers distributed arbitrarily in the 3D space, and reflectors placed close to the sector edge. The number of reflectors and scatterers contributing to the received signal depends on the UE position. If the received power via some cluster is less than 10% of the LOS power at that position, this cluster is ignored. Accordingly, the complex channel gain of the $m^{\rm th}$ path is modeled by $\beta_m = |\beta_m| e^{j\vartheta_m}$ such that

$$|\beta_m|^2 = \frac{\lambda^2}{(4\pi)^2} \begin{cases} 1/D_1^2 & \text{LOS} \\ \Gamma_{\rm R}/(d_{1,m} + d_{2,m})^2 & \text{reflector} \\ \sigma_{\rm RCS}^2/(4\pi (d_{1,m} d_{2,m})^2) & \text{scatterer,} \end{cases} \tag{44}$$

where $\vartheta_1 = 2\pi D_1/\lambda$ and $\vartheta_m = 2\pi(d_{1,m} + d_{2,m})/\lambda$ for $m > 1$, while $\sigma^2_{\mathrm{RCS}} = 50$ m^2, and $\Gamma_{\mathrm{R}} = 0.7$ are the radar cross section, and the reflection coefficient, respectively. The locations of reflectors are computed using the virtual transmitter method [30]. We consider 5 scenarios, for each of which we evaluate the PEB and OEB:

1) *LOS*: Free space propagation only, without NLOS paths.
2) *LOS+R*: A LOS path and $M-1$ reflected NLOS paths.
3) *LOS+S*: A LOS path and $M-1$ scattered NLOS paths.
4) *LOS+C*: A LOS path and a mix of both scattered and reflected NLOS paths.
5) *NLOS*: The LOS path is blocked, so only scattered and reflected NLOS paths exist.

All the following results are obtained with $N_{\mathrm{B}} = 25$, $N_{\mathrm{T}} = N_{\mathrm{R}} = 144$, unless otherwise stated.

B. Downlink PEB and OEB

Fig. 6 (left) shows the downlink PEB and OEB as a function of the UE location for the LOS case with the BS located at $(0, 0)$. With $N_{\mathrm{T}} = N_{\mathrm{R}} = 144$, and $N_{\mathrm{B}} = 25$, the maximum PEB in the sector is 40 cm, while the maximum OEB is 1° in the LOS scenario. Note that from (42b), the PEB increases with $\|\mathbf{p}\|$. This explains the yellow area around the corners. Moreover, the closer the UE to the BS, i.e., as $\theta_{\mathrm{BS}} \to \pi$, singularities appear in the FIM, and the OEB tends to worsen, hence the yellow areas around the BS. Scatterers and reflectors are introduced in the 3D space, so that a maximum of 5 clusters contribute at any given location. Based on that, Fig. 6 (right) shows the PEB and OEB for the LOS+C case. Although incorporating NLOS clusters in the localization does not lower the maximum bound value, it improves the bounds at those locations where the clusters' signal are received. In the illustrated example, the clusters mainly affect the top and center areas of the sector. Finally, note the yellow dots in the central area of the PEB and OEB (LOS+C). These dots occur because at these locations, the scatterer blocks the LOS, violating the unique parameters assumption, and causing singularities in the FIM.

To obtain a more concise and quantitative assessment of the performance, we collect all the PEB and OEB values across the space and visualize them in a cumulative distribution function (CDF). Subsequently, Fig. 7 is obtained for all 5 considered scenarios, where only PEB is shown, as the curves look similar for OEB. The PEB obtained from the approximate approache, is also shown in the figure. We observe the following: overall, scatterers and/or reflectors improve the localization performance, compared to the LOS-only scenario, despite the fact that more parameters need to be estimated. Scatterers are mainly useful in providing very low PEB for

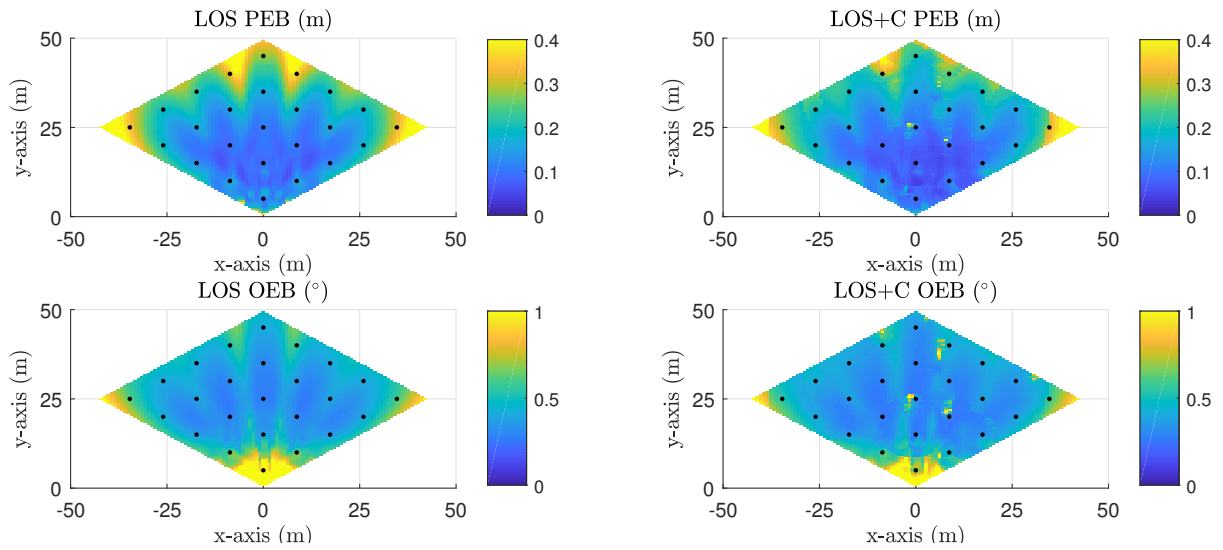

Fig. 6. PEB and OEB for downlink LOS (left) and LOS+C (right). The black dots denote the centers of beams, $N_{\mathrm{B}} = 25$.

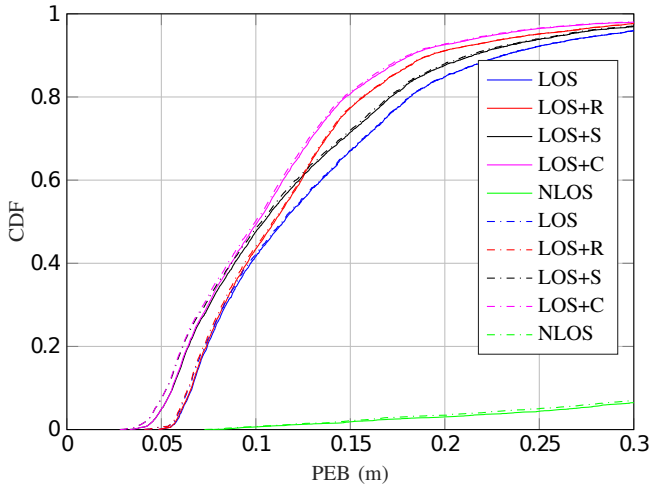

Fig. 7. The CDF of downlink PEB for different scenarios using the exact (solid) and approximate (dashed) FIM approaches.

very few locations, while reflectors can provide modest improvement for many locations. When scatterers and reflectors are combined, we see both phenomena. It is also apparent that the approximate approaches closely follow the exact PEB and OEB and that the approximation always leads to a slightly lower PEB and OEB, due to the independent paths assumption, under this approach. Note that at a 90% CDF, the PEB values for LOS, LOS+R, LOS+S, LOS+C are 0.23 m, 0.21 m, 0.19 m and 0.18 m, respectively. Finally, note that the NLOS scenario is unreliable, with a PEB of 0.5 m at a 13% CDF.

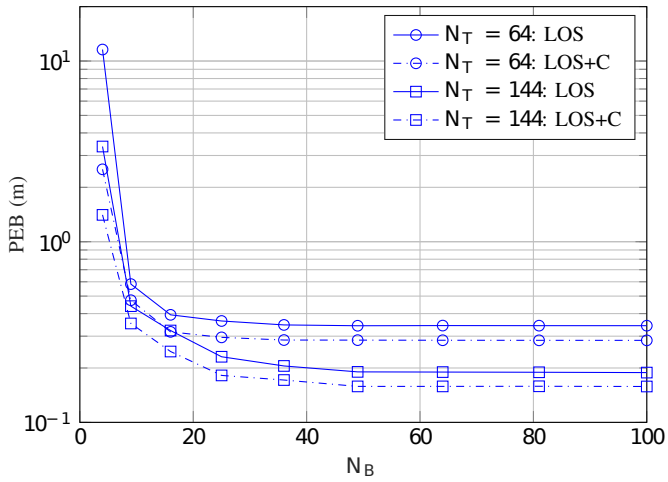

Fig. 8. Saturation effect of the downlink PEB w.r.t N_{B} with $N_{\mathrm{T}} \in \{64, 144\}$, for LOS and LOS+C, at $\mathrm{CDF} = 0.9$

C. The Selection of N_{B}

In this section, we will evaluate the impact of the number of beams on downlink localization. Considering directional beamforming and a given number of transmit antennas, i.e., a fixed beamwidth, the selection of N_{B} becomes a trade-off between hardware complexity and the coverage area up to a certain value of N_{B}, where more beams do not necessarily assist the localization. This relationship is highlighted in Fig. 8 for PEB values across the space, at a CDF of 90% (similar results hold for the OEB, not shown). It can be seen that at a small N_{B}, the bounds are high, but as N_{B} increases, the bounds start to decrease due better coverage. However, as N_{B} continues to increase, the bounds reach a floor and adding more beams only adds more complexity while providing negligible improvement. This is because the total transmit power must be divided over more beams, so as soon as the area is covered, more beams do not improve performance. This also means that the number of beams should be selected as a function of the beamwidth. For instance, considering $N_{\mathrm{T}} \in \{64, 144\}$, beams with $N_{\mathrm{T}} = 64$ are wider than $N_{\mathrm{T}} = 144$, and thus wider beams provide better coverage for a fixed value of N_{B}. This is why, in this case, it is sufficient to have 9 beams for $N_{\mathrm{T}} = 64$, compared to 25 beams in the case of $N_{\mathrm{T}} = 144$. Finally, note that this trade-off does not depend on whether clusters exist or not.

D. Downlink vs. Uplink Comparison

We now compare uplink and downlink in terms of the following parameters: (i) UE orientation; (ii) number of transmit antennas; (iii) number of receive antennas. We recall that in the downlink,

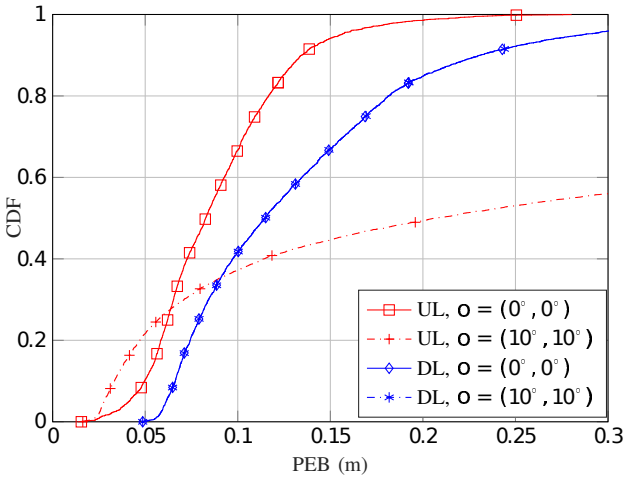

Fig. 9. CDF of the PEB over the entire sector, for uplink and downlink, with different orientation angles.

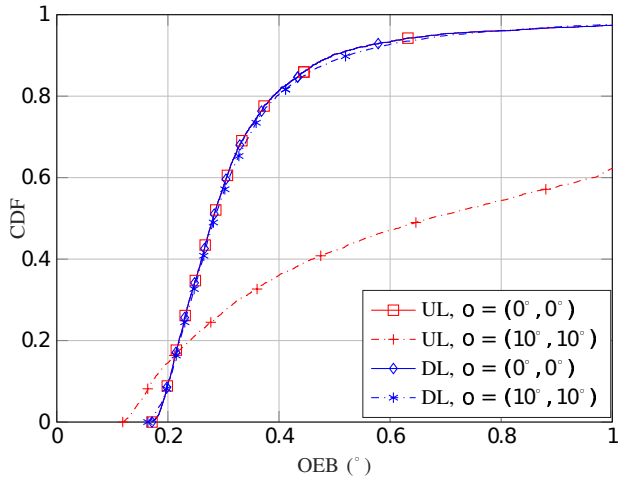

Fig. 10. CDF of the OEB over the entire sector, for uplink and downlink, with different orientation angles.

the transmitter (BS) has a known position and orientation, while in the uplink, the transmitter (UE) has an unknown position and orientation.

1) UE Orientation impact on PEB and OEB: Considering Fig. 9, the CDF of PEB is shown for uplink and downlink with two different UE orientation angles. Since the *downlink PEB* is independent of the UE orientation, the downlink PEB is identical in both $0°$ and $10°$ orientation cases. on the contrary, the *uplink PEB* is highly dependent on the UE orientation: beamforming from the UE is performed in fixed directions in the UE's frame of reference. Depending on the UE location, beams may miss the BS. With $10°$ orientation, this happens more frequently, thus degrading the PEB. Finally, although in this example the uplink with $0°$ orientation is better than the downlink in Fig. 9, this is not alway the case. In fact, this depends on the choice of N_{R}, as will be demonstrated.

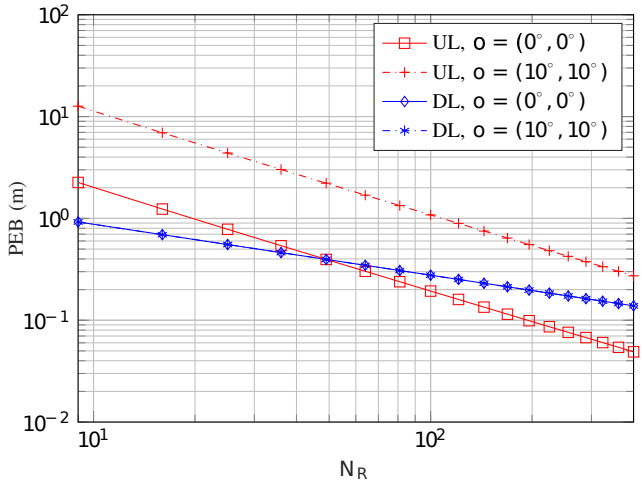

Fig. 11. Scaling of the PEB w.r.t N_{R} for uplink and downlink LOS scenarios, at $\mathrm{CDF} = 0.9$, with different orientation angles.

For the OEB in Fig. 10, downlink curves again coincide, with the uplink OEB for 0° yielding similar performance. This is due to OEB being a function of DOA and DOD, which are interchangeable when UE and BS have the same orientation. However, when the UE orientation is 10°, OEB is again degraded, similar to the PEB.

2) Effect of N_{R} and N_{T}: Fig. 11 shows the scaling effect of the PEB at 90% CDF for LOS, which in line with Table I, implies that uplink and downlink have different scaling exponents. This leads the two lines to cross at some value. So, regarding PEB, choosing N_{R} on either side of this crossing point dictates the outperforming scheme, uplink or downlink. Specifically, for very large number of receive antennas, uplink PEB becomes far better than downlink PEB.

From Table I, however, the OEB scaling is different than PEB. This is confirmed by the results of the OEB at 90% CDF for LOS shown in Fig. 12. It can be seen that for relatively large N_{R}, OEB scales of $1/\sqrt{N_{\mathrm{R}}}$, while for small N_{R}, it scales of $1/N_{\mathrm{R}}$, in both uplink and downlink.

Finally, we discuss the effect of N_{T} on the PEB shown in Fig. 13 (similar OEB results are observed, not shown). Both PEB and OEB scale non-linearly with N_{T}. Small N_{T} results in bad performance due to less spatial resolution and lower SNR. As N_{T} increases, the SNR increases but the beamwidth decreases. At a certain point, the beams become too narrow and bounds start to worsen. Both uplink and downlink suffer from this effect, but it is more severe in the uplink.

VI. Conclusions

In this paper, we have considered mmWave localization performance limits in terms of PEB and OEB, for uplink and downlink localization with arbitrary array geometries in multipath environments. We have investigated these two bounds using exact and approximate approaches,

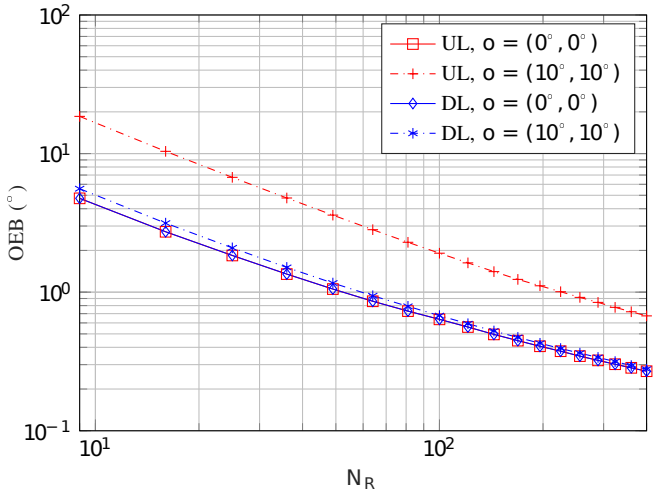

Fig. 12. Scaling of the OEB w.r.t N_{R} for uplink and downlink LOS scenarios, at $\mathrm{CDF} = 0.9$, with different orientation angles.

tailored to mmWave communication. The latter is obtained by decomposing the multipath EFIM of position and orientation into multiple single path FIMs. Focusing on outdoor scenarios, our simulations show that the NLOS clusters improve the localization when a LOS path exists and that localization in the absence of LOS is possible, though with severe performance penalties. We have analyzed the impact of the number of beams, as well as the number of transmit and receive antennas. Even though having many receive antennas is more beneficial in uplink localization than in downlink localization, the former is generally harder since transmit beamforming at UE may point in directions that are not useful for localization.

APPENDIX A
EXACT CHANNEL PARAMETERS FIM SUBMATRICES

The entries of (9) are given by

$$\mathbf{J}_{\boldsymbol{\theta}_{\mathrm{T}}\boldsymbol{\theta}_{\mathrm{T}}} = \gamma\Re\{(\mathbf{B}^{\mathrm{H}}\mathbf{A}_{\mathrm{R}}^{\mathrm{H}}\mathbf{A}_{\mathrm{R}}\mathbf{B}) \odot (\mathbf{K}_{\mathrm{T}}^{\mathrm{H}}\mathbf{F}\mathbf{F}^{\mathrm{H}}\mathbf{K}_{\mathrm{T}})^{\mathrm{T}} \odot \mathbf{R}_0\}, \tag{45a}$$

$$\mathbf{J}_{\boldsymbol{\phi}_{\mathrm{R}}\boldsymbol{\phi}_{\mathrm{R}}} = \gamma\Re\{(\mathbf{B}^{\mathrm{H}}\mathbf{P}_{\mathrm{R}}^{\mathrm{H}}\mathbf{P}_{\mathrm{R}}\mathbf{B}) \odot (\mathbf{A}_{\mathrm{T}}^{\mathrm{H}}\mathbf{F}\mathbf{F}^{\mathrm{H}}\mathbf{A}_{\mathrm{T}})^{\mathrm{T}} \odot \mathbf{R}_0\}, \tag{45b}$$

$$\mathbf{J}_{\boldsymbol{\phi}_{\mathrm{T}}\boldsymbol{\phi}_{\mathrm{T}}} = \gamma\Re\{(\mathbf{B}^{\mathrm{H}}\mathbf{A}_{\mathrm{R}}^{\mathrm{H}}\mathbf{A}_{\mathrm{R}}\mathbf{B}) \odot (\mathbf{P}_{\mathrm{T}}^{\mathrm{H}}\mathbf{F}\mathbf{F}^{\mathrm{H}}\mathbf{P}_{\mathrm{T}})^{\mathrm{T}} \odot \mathbf{R}_0\}, \tag{45c}$$

$$\mathbf{J}_{\boldsymbol{\beta}_{\mathrm{R}}\boldsymbol{\beta}_{\mathrm{R}}} = \mathbf{J}_{\boldsymbol{\beta}_{\mathrm{I}}\boldsymbol{\beta}_{\mathrm{I}}} = \Re\{(\mathbf{A}_{\mathrm{R}}^{\mathrm{H}}\mathbf{A}_{\mathrm{R}}) \odot (\mathbf{A}_{\mathrm{T}}^{\mathrm{H}}\mathbf{F}\mathbf{F}^{\mathrm{H}}\mathbf{A}_{\mathrm{T}})^{\mathrm{T}} \odot \mathbf{R}_0\}, \tag{45d}$$

$$\mathbf{J}_{\boldsymbol{\tau}\boldsymbol{\tau}} = \gamma\Re\{(\mathbf{B}^{\mathrm{H}}\mathbf{A}_{\mathrm{R}}^{\mathrm{H}}\mathbf{A}_{\mathrm{R}}\mathbf{B}) \odot (\mathbf{A}_{\mathrm{T}}^{\mathrm{H}}\mathbf{F}\mathbf{F}^{\mathrm{H}}\mathbf{A}_{\mathrm{T}})^{\mathrm{T}} \odot \mathbf{R}_2\}, \tag{45e}$$

$$\mathbf{J}_{\boldsymbol{\theta}_{\mathrm{R}}\boldsymbol{\theta}_{\mathrm{T}}} = \gamma\Im\{j(\mathbf{B}^{\mathrm{H}}\mathbf{K}_{\mathrm{R}}{}^{\mathrm{H}}\mathbf{A}_{\mathrm{R}}\mathbf{B}) \odot (\mathbf{K}_{\mathrm{T}}^{\mathrm{H}}\mathbf{F}\mathbf{F}^{\mathrm{H}}\mathbf{A}_{\mathrm{T}})^{\mathrm{T}} \odot \mathbf{R}_0\}, \tag{45f}$$

$$\mathbf{J}_{\boldsymbol{\theta}_{\mathrm{R}}\boldsymbol{\phi}_{\mathrm{R}}} = \gamma\Re\{(\mathbf{B}^{\mathrm{H}}\mathbf{K}_{\mathrm{R}}^{\mathrm{H}}\mathbf{P}_{\mathrm{R}}\mathbf{B}) \odot (\mathbf{A}_{\mathrm{T}}^{\mathrm{H}}\mathbf{F}\mathbf{F}^{\mathrm{H}}\mathbf{A}_{\mathrm{T}})^{\mathrm{T}} \odot \mathbf{R}_0\}, \tag{45g}$$

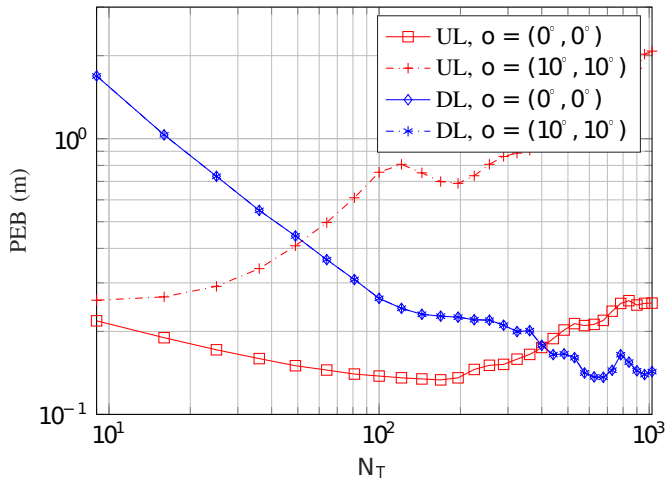

Fig. 13. Scaling of the PEB w.r.t N_{T} for uplink and downlink LOS scenarios, at CDF $= 0.9$, with different orientation angles.

$$\mathbf{J}_{\boldsymbol{\theta}_{\mathrm{R}}\boldsymbol{\phi}_{\mathrm{T}}} = \gamma\Im\{j(\mathbf{B}^{\mathrm{H}}\mathbf{K}_{\mathrm{R}}{}^{\mathrm{H}}\mathbf{A}_{\mathrm{R}}\mathbf{B}) \odot (\mathbf{P}_{\mathrm{T}}^{\mathrm{H}}\mathbf{F}\mathbf{F}^{\mathrm{H}}\mathbf{A}_{\mathrm{T}})^{\mathrm{T}} \odot \mathbf{R}_0\}, \tag{45h}$$

$$\mathbf{J}_{\boldsymbol{\theta}_{\mathrm{T}}\boldsymbol{\phi}_{\mathrm{R}}} = \gamma\Im\{j(\mathbf{B}^{\mathrm{H}}\mathbf{A}_{\mathrm{R}}^{\mathrm{H}}\mathbf{P}_{\mathrm{R}}\mathbf{B}) \odot (\mathbf{A}_{\mathrm{T}}^{\mathrm{H}}\mathbf{F}\mathbf{F}^{\mathrm{H}}\mathbf{K}_{\mathrm{T}})^{\mathrm{T}} \odot \mathbf{R}_0\}, \tag{45i}$$

$$\mathbf{J}_{\boldsymbol{\theta}_{\mathrm{T}}\boldsymbol{\phi}_{\mathrm{T}}} = \gamma\Re\{(\mathbf{B}^{\mathrm{H}}\mathbf{A}_{\mathrm{R}}^{\mathrm{H}}\mathbf{A}_{\mathrm{R}}\mathbf{B}) \odot (\mathbf{P}_{\mathrm{T}}^{\mathrm{H}}\mathbf{F}\mathbf{F}^{\mathrm{H}}\mathbf{K}_{\mathrm{T}})^{\mathrm{T}} \odot \mathbf{R}_0\}, \tag{45j}$$

$$\mathbf{J}_{\boldsymbol{\phi}_{\mathrm{R}}\boldsymbol{\phi}_{\mathrm{T}}} = \gamma\Im\{j(\mathbf{B}^{\mathrm{H}}\mathbf{P}_{\mathrm{R}}^{\mathrm{H}}\mathbf{A}_{\mathrm{R}}\mathbf{B}) \odot (\mathbf{P}_{\mathrm{T}}^{\mathrm{H}}\mathbf{F}\mathbf{F}^{\mathrm{H}}\mathbf{A}_{\mathrm{T}})^{\mathrm{T}} \odot \mathbf{R}_0\}, \tag{45k}$$

$$\mathbf{J}_{\boldsymbol{\beta}_{\mathrm{R}}\boldsymbol{\beta}_{\mathrm{I}}} = \gamma\Re\{j(\mathbf{A}_{\mathrm{R}}^{\mathrm{H}}\mathbf{A}_{\mathrm{R}}) \odot (\mathbf{A}_{\mathrm{T}}^{\mathrm{H}}\mathbf{F}\mathbf{F}^{\mathrm{H}}\mathbf{A}_{\mathrm{T}})^{\mathrm{T}} \odot \mathbf{R}_0\}, \tag{45l}$$

$$\mathbf{J}_{\boldsymbol{\theta}_{\mathrm{R}}\boldsymbol{\tau}} = \gamma\Re\{j(\mathbf{B}^{\mathrm{H}}\mathbf{K}_{\mathrm{R}}^{\mathrm{H}}\mathbf{A}_{\mathrm{R}}\mathbf{B}) \odot (\mathbf{A}_{\mathrm{T}}^{\mathrm{H}}\mathbf{F}\mathbf{F}^{\mathrm{H}}\mathbf{A}_{\mathrm{T}})^{\mathrm{T}} \odot \mathbf{R}_1\}, \tag{45m}$$

$$\mathbf{J}_{\boldsymbol{\theta}_{\mathrm{T}}\boldsymbol{\tau}} = \gamma\Im\{(\mathbf{B}^{\mathrm{H}}\mathbf{A}_{\mathrm{R}}^{\mathrm{H}}\mathbf{A}_{\mathrm{R}}\mathbf{B}) \odot (\mathbf{A}_{\mathrm{T}}^{\mathrm{H}}\mathbf{F}\mathbf{F}^{\mathrm{H}}\mathbf{K}_{\mathrm{T}})^{\mathrm{T}} \odot \mathbf{R}_1\}, \tag{45n}$$

$$\mathbf{J}_{\boldsymbol{\phi}_{\mathrm{R}}\boldsymbol{\tau}} = \gamma\Re\{j(\mathbf{B}^{\mathrm{H}}\mathbf{P}_{\mathrm{R}}^{\mathrm{H}}\mathbf{A}_{\mathrm{R}}\mathbf{B}) \odot (\mathbf{A}_{\mathrm{T}}^{\mathrm{H}}\mathbf{F}\mathbf{F}^{\mathrm{H}}\mathbf{A}_{\mathrm{T}})^{\mathrm{T}} \odot \mathbf{R}_1\}, \tag{45o}$$

$$\mathbf{J}_{\boldsymbol{\phi}_{\mathrm{T}}\boldsymbol{\tau}} = \gamma\Im\{(\mathbf{B}^{\mathrm{H}}\mathbf{A}_{\mathrm{R}}^{\mathrm{H}}\mathbf{A}_{\mathrm{R}}\mathbf{B}) \odot (\mathbf{A}_{\mathrm{T}}^{\mathrm{H}}\mathbf{F}\mathbf{F}^{\mathrm{H}}\mathbf{P}_{\mathrm{T}})^{\mathrm{T}} \odot \mathbf{R}_1\}, \tag{45p}$$

$$\mathbf{J}_{\boldsymbol{\theta}_{\mathrm{R}}\boldsymbol{\beta}_{\mathrm{I}}} + j\mathbf{J}_{\boldsymbol{\theta}_{\mathrm{R}}\boldsymbol{\beta}_{\mathrm{R}}} = -\gamma\ (\mathbf{B}^{\mathrm{H}}\mathbf{K}_{\mathrm{R}}^{\mathrm{H}}\mathbf{A}_{\mathrm{R}}) \odot (\mathbf{A}_{\mathrm{T}}^{\mathrm{H}}\mathbf{F}\mathbf{F}^{\mathrm{H}}\mathbf{A}_{\mathrm{T}})^{\mathrm{T}} \odot \mathbf{R}_0, \tag{45q}$$

$$\mathbf{J}_{\boldsymbol{\theta}_{\mathrm{T}}\boldsymbol{\beta}_{\mathrm{I}}} + j\mathbf{J}_{\boldsymbol{\theta}_{\mathrm{T}}\boldsymbol{\beta}_{\mathrm{R}}} = \gamma\ (\mathbf{B}^{\mathrm{H}}\mathbf{A}_{\mathrm{R}}^{\mathrm{H}}\mathbf{A}_{\mathrm{R}}) \odot (\mathbf{A}_{\mathrm{T}}^{\mathrm{H}}\mathbf{F}\mathbf{F}^{\mathrm{H}}\mathbf{K}_{\mathrm{T}})^{\mathrm{T}} \odot \mathbf{R}_0, \tag{45r}$$

$$\mathbf{J}_{\boldsymbol{\phi}_{\mathrm{R}}\boldsymbol{\beta}_{\mathrm{I}}} + j\mathbf{J}_{\boldsymbol{\phi}_{\mathrm{R}}\boldsymbol{\beta}_{\mathrm{R}}} = -\gamma\ (\mathbf{B}^{\mathrm{H}}\mathbf{P}_{\mathrm{R}}^{\mathrm{H}}\mathbf{A}_{\mathrm{R}}) \odot (\mathbf{A}_{\mathrm{T}}^{\mathrm{H}}\mathbf{F}\mathbf{F}^{\mathrm{H}}\mathbf{A}_{\mathrm{T}})^{\mathrm{T}} \odot \mathbf{R}_0, \tag{45s}$$

$$\mathbf{J}_{\boldsymbol{\phi}_{\mathrm{T}}\boldsymbol{\beta}_{\mathrm{I}}} + j\mathbf{J}_{\boldsymbol{\phi}_{\mathrm{T}}\boldsymbol{\beta}_{\mathrm{R}}} = \gamma\ (\mathbf{B}^{\mathrm{H}}\mathbf{A}_{\mathrm{R}}^{\mathrm{H}}\mathbf{A}_{\mathrm{R}}) \odot (\mathbf{A}_{\mathrm{T}}^{\mathrm{H}}\mathbf{F}\mathbf{F}^{\mathrm{H}}\mathbf{P}_{\mathrm{T}})^{\mathrm{T}} \odot \mathbf{R}_0, \tag{45t}$$

$$\mathbf{J}_{\boldsymbol{\beta}_{\mathrm{R}}\boldsymbol{\tau}} + j\mathbf{J}_{\boldsymbol{\beta}_{\mathrm{I}}\boldsymbol{\tau}} = \gamma\ (\mathbf{A}^{\mathrm{H}}\mathbf{A}_{\mathrm{R}}\mathbf{B}) \odot (\mathbf{A}_{\mathrm{T}}^{\mathrm{H}}\mathbf{F}\mathbf{F}^{\mathrm{H}}\mathbf{A}_{\mathrm{T}})^{\mathrm{T}} \odot \mathbf{R}_1, \tag{45u}$$

Appendix B
CRLBs of Single-Path Parameters

Directly from (24), it is easy to see that

$$\mathrm{CRLB}(\tau) = \frac{1}{4\gamma\pi^2|\beta|^2 G W_{\mathrm{eff}}^2}. \tag{46}$$

The FIM of $\boldsymbol{\varphi}_{\boldsymbol{\theta},\boldsymbol{\phi},\boldsymbol{\beta}} \triangleq [\theta_{\mathrm{R}}, \theta_{\mathrm{T}}, \phi_{\mathrm{R}}, \phi_{\mathrm{T}}, \beta_{\mathrm{R}}, \beta_{\mathrm{I}}]^{\mathrm{T}}$ can be obtained by evaluating (9) for one path

$$\mathbf{J}_{\boldsymbol{\theta},\boldsymbol{\phi},\boldsymbol{\beta}} \triangleq \gamma|\beta|^2 \left[\begin{array}{c:c} \mathbf{A} & \mathbf{U} \\ \hdashline \mathbf{U}^{\mathrm{T}} & \mathbf{C} \end{array}\right] = \gamma|\beta|^2 \left[\begin{array}{cccc:cc} R_\theta G & 0 & X_{\theta,\phi} G & 0 & 0 & 0 \\ 0 & T_\theta & 0 & Y'_{\theta,\phi} & S_1 & U_1 \\ X_{\theta,\phi} G & 0 & R_\phi G & 0 & 0 & 0 \\ 0 & Y'_{\theta,\phi} & 0 & T_\phi & S_2 & U_2 \\ \hdashline 0 & S_1 & 0 & S_2 & \frac{G}{|\beta|^2} & 0 \\ 0 & U_1 & 0 & U_2 & 0 & \frac{G}{|\beta|^2} \end{array}\right], \tag{47}$$

where $S_1 \triangleq -\Im\{\beta V_\theta\}/|\beta|^2, U_1 \triangleq \Re\{\beta V_\theta\}/|\beta|^2$, $S_2 \triangleq -\Im\{\beta V_\phi\}/|\beta|^2$, and $U_2 \triangleq \Re\{\beta V_\phi\}/|\beta|^2$. Then, we compute the CRLBs of DOA and DOD using their EFIM as

$$\mathbf{J}^{\mathrm{e}}_{\boldsymbol{\theta},\boldsymbol{\phi}} = \mathbf{A} - \mathbf{U}\mathbf{C}^{-1}\mathbf{U}^{\mathrm{T}} = \gamma|\beta|^2 \begin{bmatrix} R_\theta G & 0 & X_{\theta,\phi} G & 0 \\ 0 & \frac{L_\theta}{G} & 0 & \frac{Y_{\theta,\phi}}{G} \\ X_{\theta,\phi} G & 0 & R_\phi G & 0 \\ 0 & \frac{Y_{\theta,\phi}}{G} & 0 & \frac{L_\phi}{G} \end{bmatrix}. \tag{48}$$

To simplify the inverse computation, we utilize the independence between DOA and DOD to re-order $\mathbf{J}^{\mathrm{e}}_{\boldsymbol{\theta},\boldsymbol{\phi}}$ to write (49), from which (26) follow.

$$\mathrm{CRLB}\left((\theta_{\mathrm{R}}, \phi_{\mathrm{R}})\right) = \frac{1}{\gamma|\beta|^2 G} \begin{bmatrix} R_\theta & X_{\theta,\phi} \\ X_{\theta,\phi} & R_\phi \end{bmatrix}^{-1}, \tag{49a}$$

$$\mathrm{CRLB}\left((\theta_{\mathrm{T}}, \phi_{\mathrm{T}})\right) = \frac{G}{\gamma|\beta|^2} \begin{bmatrix} L_\theta & Y_{\theta,\phi} \\ Y_{\theta,\phi} & L_\phi \end{bmatrix}^{-1}, \tag{49b}$$

APPENDIX C
SPECIAL CASES: URA AND ULA PARAMETERS

A. Example – URA and 3D Channel

To compute the CRLBs, PEB or OEB for URA, in this section, we specify the parameters of (24) assuming that the receiver array is located in xz-plane, such that normalized element locations are given by $\mathbf{x}_{\mathrm{R}} = (\mathbf{1}^{\mathrm{T}}_{N_{\mathrm{R},z}} \otimes \mathbf{x}^{(1)}_{\mathrm{R}})/d$, $\mathbf{y}_{\mathrm{R}} = \mathbf{0}_{N_{\mathrm{R}}}$, and $\mathbf{z}_{\mathrm{R}} = (\mathbf{z}^{(1)}_{\mathrm{R}} \otimes \mathbf{1}^{\mathrm{T}}_{N_{\mathrm{R},x}})/d$, where $\mathbf{1}_N$ is vector of ones with length N, $\otimes$ denotes the Kronecker product, $N_{\mathrm{R},x}$, $N_{\mathrm{R},z}$ are the number of antennas in the x and z directions, respectively, such that $N_{\mathrm{R}} = N_{\mathrm{R},x} N_{\mathrm{R},z}$, and d is the antenna spacing. Moreover $\mathbf{x}^{(1)}_{\mathrm{R}}$ and $\mathbf{z}^{(1)}_{\mathrm{R}}$ are the coordinates of the ULA lying in the x-axis and z-axis, respectively, such that $x^{(1)}_{\mathrm{R},n} = (n - (N_{\mathrm{R},x} - 1)/2)d, \quad n = 0, 1, ...N_{\mathrm{R},x} - 1$,

$z^{(1)}_{\mathrm{R},n} = (n-(N_{\mathrm{R},z}-1)/2)d, \quad n=0,1,...N_{\mathrm{R},z}-1$. From (12c), we write

$$\tilde{\mathbf{K}}_{\mathrm{R}} = \frac{2\pi d}{\lambda}\,\mathrm{diag}(\cos\theta_{\mathrm{R}}\cos\phi_{\mathrm{R}}\mathbf{x}_{\mathrm{R}} - \sin\theta_{\mathrm{R}}\mathbf{z}_{\mathrm{R}}), \tag{50a}$$

$$\tilde{\mathbf{P}}_{\mathrm{R}} = -\frac{2\pi d}{\lambda}\sin\theta_{\mathrm{R}}\sin\phi_{\mathrm{R}}\,\mathrm{diag}(\mathbf{x}_{\mathrm{R}}), \tag{50b}$$

Defining $\alpha \triangleq 4\pi^2 d^2/\lambda^2$, and assuming $(N^2_{\mathrm{R},z}-1) \approx N^2_{\mathrm{R},z}$ and $(N^2_{\mathrm{R},x}-1) \approx N^2_{\mathrm{R},x}$, then $\mathbf{x}^{\mathrm{T}}_{\mathrm{R}}\mathbf{x}_{\mathrm{R}} = N_{\mathrm{R}}N^2_{\mathrm{R},x}/12, \mathbf{z}^{\mathrm{T}}_{\mathrm{R}}\mathbf{z}_{\mathrm{R}} = N_{\mathrm{R}}N^2_{\mathrm{R},z}/12$. As a result, it can be verified that,

$$X_{\theta,\phi} = \frac{\mathrm{Tr}(\tilde{\mathbf{K}}_{\mathrm{R}}\tilde{\mathbf{P}}_{\mathrm{R}})}{N_R} = -\frac{\alpha}{12}\cos\theta_{\mathrm{R}}\cos\phi_{\mathrm{R}}\sin\theta_{\mathrm{R}}\sin\phi_{\mathrm{R}}N^2_{\mathrm{R},z}, \tag{51a}$$

$$R_\theta = \frac{\mathrm{Tr}(\tilde{\mathbf{K}}^2_{\mathrm{R}})}{N_R} = \frac{\alpha}{12}\big(\cos^2\theta_{\mathrm{R}}\cos^2\phi_{\mathrm{R}}N^2_{\mathrm{R},x} + \sin^2\theta_{\mathrm{R}}N^2_{\mathrm{R},z}\big), \tag{51b}$$

$$R_\phi = \frac{\mathrm{Tr}(\tilde{\mathbf{P}}^2_{\mathrm{R}})}{N_R} = \frac{\alpha}{12}\sin^2\theta_{\mathrm{R}}\sin^2\phi_{\mathrm{R}}N^2_{\mathrm{R},x}. \tag{51c}$$

To compute the transmitter-side parameters, define $\mathbf{X}_{\mathrm{T}} = \mathrm{diag}(\mathbf{x}_{\mathrm{T}})$, $\mathbf{Z}_{\mathrm{T}} = \mathrm{diag}(\mathbf{z}_{\mathrm{T}})$, and

$$\mathbf{M} \triangleq \begin{bmatrix} \mathbf{a}^{\mathrm{H}}_{\mathrm{T}}\mathbf{F}\mathbf{F}^{\mathrm{H}}\mathbf{a}_{\mathrm{T}} & \Re\{\mathbf{a}^{\mathrm{H}}_{\mathrm{T}}\mathbf{X}_{\mathrm{T}}\mathbf{F}\mathbf{F}^{\mathrm{H}}\mathbf{Z}_{\mathrm{T}}\mathbf{a}_{\mathrm{T}}\} \\ \mathbf{a}^{\mathrm{H}}_{\mathrm{T}}\mathbf{X}_{\mathrm{T}}\mathbf{F}\mathbf{F}^{\mathrm{H}}\mathbf{a}_{\mathrm{T}} & \mathbf{a}^{\mathrm{H}}_{\mathrm{T}}\mathbf{X}_{\mathrm{T}}\mathbf{F}\mathbf{F}^{\mathrm{H}}\mathbf{X}_{\mathrm{T}}\mathbf{a}_{\mathrm{T}} \\ \mathbf{a}^{\mathrm{H}}_{\mathrm{T}}\mathbf{Z}_{\mathrm{T}}\mathbf{F}\mathbf{F}^{\mathrm{H}}\mathbf{a}_{\mathrm{T}} & \mathbf{a}^{\mathrm{H}}_{\mathrm{T}}\mathbf{Z}_{\mathrm{T}}\mathbf{F}\mathbf{F}^{\mathrm{H}}\mathbf{Z}_{\mathrm{T}}\mathbf{a}_{\mathrm{T}} \end{bmatrix}, \tag{52}$$

Using the same procedure by which R_θ, R_ϕ, and $X_{\theta,\phi}$ are obtained, it can be shown that

$$T_\theta = \alpha\left(\cos^2\theta_{\mathrm{T}}\cos^2\phi_{\mathrm{T}}[\mathbf{M}]_{2,2} + \sin^2\theta_{\mathrm{T}}[\,\mathbf{M}]_{3,2} - 2\cos\theta_{\mathrm{T}}\cos\phi_{\mathrm{T}}\sin\theta_{\mathrm{T}}[\mathbf{M}]_{1,2}\right), \tag{53a}$$

$$V_\theta = \sqrt{\alpha}\,(\cos\theta_{\mathrm{T}}\cos\phi_{\mathrm{T}}[\mathbf{M}]_{2,1} - \sin\theta_{\mathrm{T}}[\,\mathbf{M}]_{3,1}), \tag{53b}$$

$$T_\phi = \alpha\sin^2\theta_{\mathrm{T}}\sin^2\phi_{\mathrm{T}}[\mathbf{M}]_{2,2}, \tag{53c}$$

$$V_\phi = -\sqrt{\alpha}\sin\theta_{\mathrm{T}}\sin\phi_{\mathrm{T}}[\mathbf{M}]_{2,1}, \tag{53d}$$

$$Y'_{\theta,\phi} = \alpha(-\cos\theta_{\mathrm{T}}\cos\phi_{\mathrm{T}}\sin\theta_{\mathrm{T}}\sin\phi_{\mathrm{T}}[\mathbf{M}]_{2,2} + \sin^2\theta_{\mathrm{T}}\sin\phi_{\mathrm{T}}[\mathbf{M}]_{1,2}). \tag{53e}$$

B. Example – ULA and 2D Channel

For a ULA lying on the x-axis, $\mathbf{x}_{\mathrm{R}} = \mathbf{x}^{(1)}_{\mathrm{R}}/d$, $\mathbf{y}_{\mathrm{R}} = \mathbf{z}_{\mathrm{R}} = \mathbf{0}_{N_{\mathrm{R}}}$, and $\theta_{\mathrm{R}} = \theta_{\mathrm{T}} = \pi/2$. So,

$$R_\phi = \frac{4\pi^2\sin^2\phi_{\mathrm{R}}}{\lambda^2 N_{\mathrm{R}}}\mathbf{x}^{\mathrm{T}}_{\mathrm{R}}\mathbf{x}_{\mathrm{R}} = \frac{\alpha}{12}(N^2_{\mathrm{R}}-1)\sin^2\phi_{\mathrm{R}}. \tag{54}$$

Moreover, write $\tilde{\mathbf{P}}_{\mathrm{T}} = -\sqrt{\alpha}\sin\phi_{\mathrm{T}}\mathbf{X}_{\mathrm{T}}$, then

$$T_\phi = \alpha\sin^2(\phi_{\mathrm{T}})(\mathbf{a}^{\mathrm{H}}_{\mathrm{T}}\mathbf{X}_{\mathrm{T}}\mathbf{F}\mathbf{F}^{\mathrm{H}}\mathbf{X}_{\mathrm{T}}\mathbf{a}_{\mathrm{T}}), \tag{55a}$$

$$V_\phi = -\sqrt{\alpha}\sin(\phi_{\mathrm{T}})(\mathbf{a}^{\mathrm{H}}_{\mathrm{T}}\mathbf{X}_{\mathrm{T}}\mathbf{F}\mathbf{F}^{\mathrm{H}}\mathbf{a}_{\mathrm{T}}). \tag{55b}$$

APPENDIX D
PROOF OF PROPOSITION 2

We start by deriving the EFIM of the location parameters for the m^{th} path. Then, we show that the overall EFIM can be written as a summation of the individual EFIM. For the m^{th} path,

$$\mathbf{J}^{(m)}_{\mathbf{o},\mathbf{p},\mathbf{q}_m} = \boldsymbol{\Upsilon}_m \boldsymbol{\Lambda}^{\text{e}}_m \boldsymbol{\Upsilon}^{\text{T}}_m = \begin{bmatrix} \overline{\boldsymbol{\Upsilon}}_m \boldsymbol{\Lambda}^{\text{e}}_m \overline{\boldsymbol{\Upsilon}}^{\text{T}}_m & \overline{\boldsymbol{\Upsilon}}_m \boldsymbol{\Lambda}^{\text{e}}_m \overline{\overline{\boldsymbol{\Upsilon}}}^{\text{T}}_m \\ \overline{\overline{\boldsymbol{\Upsilon}}}_m \boldsymbol{\Lambda}^{\text{e}}_m \overline{\boldsymbol{\Upsilon}}^{\text{T}}_m & \overline{\overline{\boldsymbol{\Upsilon}}} \boldsymbol{\Lambda}^{\text{e}}_m \overline{\overline{\boldsymbol{\Upsilon}}}^{\text{T}} \end{bmatrix}. \tag{56}$$

Consequently, for $\mathbf{o}$ and $\mathbf{p}$, by Schur's complement,

$$\mathbf{J}^{(m)}_{\mathbf{o},\mathbf{p}} = \overline{\boldsymbol{\Upsilon}}_m \boldsymbol{\Lambda}^{\text{e}}_m \overline{\boldsymbol{\Upsilon}}^{\text{T}}_m - \overline{\boldsymbol{\Upsilon}}_m \boldsymbol{\Lambda}^{\text{e}}_m \overline{\overline{\boldsymbol{\Upsilon}}}^{\text{T}}_m \left(\overline{\overline{\boldsymbol{\Upsilon}}} \boldsymbol{\Lambda}^{\text{e}}_m \overline{\overline{\boldsymbol{\Upsilon}}}^{\text{T}} \right)^{-1} \overline{\overline{\boldsymbol{\Upsilon}}}_m \boldsymbol{\Lambda}^{\text{e}}_m \overline{\boldsymbol{\Upsilon}}^{\text{T}}_m. \tag{57}$$

Recall that for $m = 1$ the second term above is undefined. Focusing on all the M paths, define

$$\boldsymbol{\Upsilon} \triangleq \begin{bmatrix} \overline{\boldsymbol{\Upsilon}}_1 \overline{\boldsymbol{\Upsilon}}_2 & \cdots & \overline{\boldsymbol{\Upsilon}}_M \\ \mathbf{0} & \overline{\overline{\boldsymbol{\Upsilon}}}_2 & \cdots & \mathbf{0} \\ \vdots & \vdots & \ddots & \vdots \\ \mathbf{0} & \mathbf{0} & \cdots & \overline{\overline{\boldsymbol{\Upsilon}}}_M \end{bmatrix}, \qquad \mathbf{J}^{\text{e}}_{\boldsymbol{\varphi}_{\text{CH}}} \triangleq \begin{bmatrix} \boldsymbol{\Lambda}^{\text{e}}_1 & \mathbf{0} & \cdots & \mathbf{0} \\ \mathbf{0} & \boldsymbol{\Lambda}^{\text{e}}_2 & \cdots & \mathbf{0} \\ \vdots & \vdots & \ddots & \vdots \\ \mathbf{0} & \mathbf{0} & \cdots & \boldsymbol{\Lambda}^{\text{e}}_M \end{bmatrix}. \tag{58}$$

Then from (28),

$$\mathbf{J}_{\boldsymbol{\varphi}_{\text{L}}} = \boldsymbol{\Upsilon} \mathbf{J}^{\text{e}}_{\boldsymbol{\varphi}_{\text{CH}}} \boldsymbol{\Upsilon}^{\text{T}} = \begin{bmatrix} \sum_{m=1}^{M} \overline{\boldsymbol{\Upsilon}}_m \boldsymbol{\Lambda}^{\text{e}}_m \overline{\boldsymbol{\Upsilon}}^{\text{T}}_m & \overline{\boldsymbol{\Upsilon}}_2 \boldsymbol{\Lambda}^{\text{e}}_2 \overline{\overline{\boldsymbol{\Upsilon}}}^{\text{T}}_2 & \cdots & \overline{\boldsymbol{\Upsilon}}_M \boldsymbol{\Lambda}^{\text{e}}_M \overline{\overline{\boldsymbol{\Upsilon}}}^{\text{T}}_M \\ \overline{\overline{\boldsymbol{\Upsilon}}}_2 \boldsymbol{\Lambda}^{\text{e}}_2 \overline{\boldsymbol{\Upsilon}}^{\text{T}}_2 & \overline{\overline{\boldsymbol{\Upsilon}}}_2 \boldsymbol{\Lambda}^{\text{e}}_2 \overline{\overline{\boldsymbol{\Upsilon}}}^{\text{T}}_2 & \cdots & \mathbf{0} \\ \vdots & \vdots & \ddots & \vdots \\ \overline{\overline{\boldsymbol{\Upsilon}}}_M \boldsymbol{\Lambda}^{\text{e}}_M \overline{\boldsymbol{\Upsilon}}^{\text{T}}_M & \mathbf{0} & \cdots & \overline{\overline{\boldsymbol{\Upsilon}}}_M \boldsymbol{\Lambda}^{\text{e}}_M \overline{\overline{\boldsymbol{\Upsilon}}}^{\text{T}}_M \end{bmatrix}.$$

By Schur's Complement and using (57), it is easy to verify that

$$\mathbf{J}^{\text{e}}_{\mathbf{o},\mathbf{p}} = \sum_{m=1}^{M} \overline{\boldsymbol{\Upsilon}}_m \boldsymbol{\Lambda}^{\text{e}}_m \overline{\boldsymbol{\Upsilon}}^{\text{T}}_m - \sum_{m=2}^{M} \overline{\boldsymbol{\Upsilon}}_m \boldsymbol{\Lambda}^{\text{e}}_m \overline{\overline{\boldsymbol{\Upsilon}}}^{\text{T}}_m \left(\overline{\overline{\boldsymbol{\Upsilon}}}_m \boldsymbol{\Lambda}^{\text{e}}_m \overline{\overline{\boldsymbol{\Upsilon}}}^{\text{T}}_m \right)^{-1} \overline{\overline{\boldsymbol{\Upsilon}}}_m \boldsymbol{\Lambda}^{\text{e}}_m \overline{\boldsymbol{\Upsilon}}^{\text{T}}_m, = \sum_{m=1}^{M} \mathbf{J}^{(m)}_{\mathbf{o},\mathbf{p}}. \tag{59}$$

APPENDIX E
CLOSED-FORM PEB AND OEB FOR LOS-ONLY

A. 3D localization

The EFIM of $\mathbf{o}$ and $\mathbf{p}$ can be obtained from $\mathbf{J}^{(1)}_{\mathbf{o},\mathbf{p}} = \overline{\boldsymbol{\Upsilon}}_1 \boldsymbol{\Lambda}^{\text{e}}_1 \overline{\boldsymbol{\Upsilon}}^{\text{T}}_1 \in \mathbb{R}^{5\times 5}$. From (24) and (25), the EFIM of $\boldsymbol{\theta}$, $\boldsymbol{\phi}$ and τ is given by

$$\boldsymbol{\Lambda}^{\text{e}}_1 = \begin{bmatrix} \mathbf{J}^{\text{e}}_{\boldsymbol{\theta},\boldsymbol{\phi}} & 0 \\ 0 & 4\gamma\pi^2 |\beta|^2 G W^2_{\text{eff}} \end{bmatrix}. \tag{60}$$

We consider the uplink case first. The transformation matrix for the LOS case is defined in (29)

$$\boldsymbol{\Upsilon} = \overline{\boldsymbol{\Upsilon}}_1 = \begin{bmatrix} 0 & 1 & 0 & 0 & 0 \\ 0 & 0 & 0 & -1 & 0 \\ 0 & 0 & \frac{-p_y}{p_y^2+p_x^2} & \frac{-p_y}{p_y^2+p_x^2} & \frac{p_x}{c\|\mathbf{p}\|} \\ \frac{p_z}{p_y^2+p_z^2} & \frac{-p_z}{p_y^2+p_z^2} & \frac{p_x}{p_y^2+p_x^2} & \frac{p_x}{p_y^2+p_x^2} & \frac{p_y}{c\|\mathbf{p}\|} \\ \frac{-p_y}{p_y^2+p_z^2} & \frac{p_y}{p_y^2+p_z^2} & 0 & 0 & \frac{p_z}{c\|\mathbf{p}\|} \end{bmatrix} \tag{61}$$

The derivation of PEB and OEB requires that $\mathbf{J}^{(1)}_{\mathbf{o},\mathbf{p}}$ be inverted. We achieve that by partitioning $\mathbf{J}^{(1)}_{\mathbf{o},\mathbf{p}}$ and computing the Schur's complement. Given $\mathbf{J}_{11} \in \mathbb{R}^{2\times 2}$, and $\mathbf{J}_{22} \in \mathbb{R}^{3\times 3}$, then,

$$\mathbf{J}^{(1)}_{\mathbf{o},\mathbf{p}} = \begin{bmatrix} \mathbf{J}_{11} & \mathbf{J}_{12} \\ \mathbf{J}_{12}^{\mathrm{T}} & \mathbf{J}_{22} \end{bmatrix}, \tag{62}$$

Consequently,

$$\mathrm{SPEB}_{\mathrm{UL}} = \mathrm{Tr}\left((\mathbf{J}_{22} - \mathbf{J}_{12}^{\mathrm{T}}\mathbf{J}_{11}^{-1}\mathbf{J}_{12})^{-1}\right), \tag{63a}$$

$$\mathrm{SOEB} = \mathrm{Tr}\left((\mathbf{J}_{11} - \mathbf{J}_{12}\mathbf{J}_{22}^{-1}\mathbf{J}_{12}^{\mathrm{T}})^{-1}\right). \tag{63b}$$

Writing $[p_x, p_y, p_z] = \|\mathbf{p}\|\,[\cos\phi_{\mathrm{BS}}\sin\theta_{\mathrm{BS}}, \sin\phi_{\mathrm{BS}}\sin\theta_{\mathrm{BS}}, \cos\theta_{\mathrm{BS}}]$, and recalling $\zeta_1, \tilde{\zeta}_1, \zeta_2, \tilde{\zeta}_2, A_1, A_2$ and A_3 from Section IV-C, then, simplifying the results yields

$$\mathrm{SOEB} = \; G\,\frac{L_\theta + L_\phi}{\gamma\zeta_2|\beta|^2} + \frac{R_\theta + R_\phi}{\zeta_1\gamma|\beta|^2 G}, \tag{64a}$$

$$\mathrm{SPEB}_{\mathrm{UL}} = \frac{\tilde{\zeta}_1\|\mathbf{p}\|^2}{\zeta_1\gamma|\beta|^2 G} + \frac{c^2}{4\gamma\pi^2|\beta|^2 W_{\mathrm{eff}}^2}, \tag{64b}$$

To obtain $\boldsymbol{\Upsilon}$ in the downlink, we swap the columns 1 with 2 , and 3 with 4, and repeat the same steps. It can be shown then that the downlink SOEB is idenitical to the uplink, and that

$$\mathrm{SPEB}_{\mathrm{DL}} = \frac{\tilde{\zeta}_1\|\mathbf{p}\|^2}{\zeta_1\gamma|\beta|^2 G} + \frac{c^2}{4\gamma\pi^2|\beta|^2 W_{\mathrm{eff}}^2}. \tag{65}$$

B. 2D Localization:

From (60) and (61), the 2D localization uplink case has $\tilde{\Lambda}_1 = \gamma|\beta|^2\,\mathrm{diag}\left(\begin{bmatrix} R_\phi G & \frac{L_\phi}{G} & 4\pi^2 G W_{\mathrm{eff}}^2 \end{bmatrix}\right)$

$$\boldsymbol{\Upsilon} = \begin{bmatrix} 0 & -1 & 0 \\ \frac{-\sin\theta_{\mathrm{BS}}}{\|\mathbf{p}\|} & \frac{-\sin\theta_{\mathrm{BS}}}{\|\mathbf{p}\|} & \frac{\cos\theta_{\mathrm{BS}}}{c} \\ \frac{\cos\theta_{\mathrm{BS}}}{\|\mathbf{p}\|} & \frac{\cos\theta_{\mathrm{BS}}}{\|\mathbf{p}\|} & \frac{\sin\theta_{\mathrm{BS}}}{c} \end{bmatrix}. \tag{66}$$

Thus, it can be shown that $\mathbf{J}_{11} = L_\phi$, $\mathbf{J}_{12} = \frac{L_\phi}{\|\mathbf{p}\|}\begin{bmatrix}\sin\theta_{\rm BS} & -\cos\theta_{\rm BS}\end{bmatrix}$, and

$$\mathbf{J}_{22} = \frac{(L_\phi + R_\phi G^2)}{\|\mathbf{p}\|^2}\begin{bmatrix}\sin^2\theta_{\rm BS} & -\sin\theta_{\rm BS}\cos\theta_{\rm BS}\\ -\sin\theta_{\rm BS}\cos\theta_{\rm BS} & \sin^2\theta_{\rm BS}\end{bmatrix} + \frac{4\pi^2 G^2 W_{\rm eff}^2}{c^2}\begin{bmatrix}\cos^2\theta_{\rm BS} & \sin\theta_{\rm BS}\cos\theta_{\rm BS}\\ \sin\theta_{\rm BS}\cos\theta_{\rm BS} & \sin^2\theta_{\rm BS}\end{bmatrix}.$$

Consequently, it follows from (63b) that

$$\mathrm{SOEB} = \frac{G}{\gamma|\beta|^2}\left(L_\phi - \frac{L_\phi^2}{\|\mathbf{p}\|^2\det(\mathbf{J}_{22})}\left(\frac{4\pi^2 G^2 W_{\rm eff}^2}{c^2}\right)\right)^{-1} \tag{67}$$

where $\det(\mathbf{J}_{22}) = (L_\phi + R_\phi G^2)\frac{4\pi^2 W^2 G^2}{3c^2\|\mathbf{p}\|^2}$. Finally, it is straight-forward that

$$\mathrm{SOEB} = \frac{1}{\gamma|\beta|^2}\left(\frac{1}{R_\phi G} + \frac{G}{L_\phi}\right), \tag{68}$$

which leads to (43a). Similarly, from (63a) it can be show that

$$\mathrm{SPEB}_{\rm UL} = \frac{1}{\gamma|\beta|^2}\left(\frac{\|\mathbf{p}\|^2}{R_\phi G} + \frac{c^2}{4\pi^2 G W_{\rm eff}^2}\right). \tag{69}$$

Repeating the same steps after swapping the first and second columns of $\boldsymbol{\Upsilon}$ yields

$$\mathrm{SPEB}_{\rm DL} = \frac{1}{\gamma|\beta|^2}\left(\frac{G\|\mathbf{p}\|^2}{L_\phi} + \frac{c^2}{4\pi^2 G W_{\rm eff}^2}\right). \tag{70}$$

REFERENCES

[1] J. G. Andrews, S. Buzzi, W. Choi, S. V. Hanly, A. Lozano, A. Soong, and J. C. Zhang, "What will 5G be?" *IEEE J. Sel. Areas Commun.*, vol. 32, no. 6, pp. 1065–1082, June 2014.

[2] Z. Pi and F. Khan, "An introduction to millimeter-wave mobile broadband systems," *IEEE Commun. Mag*, vol. 49, no. 6, pp. 101–107, June 2011.

[3] T. S. Rappaport, S. Sun, R. Mayzus, H. Zhao, Y. Azar, K. Wang, G. N. Wong, J. K. Schulz, M. Samimi, and F. Gutierrez, "Millimeter wave mobile commun. for 5G cellular: It will work!" *IEEE Access*, vol. 1, pp. 335–349, 2013.

[4] R. W. Heath, N. Gonzlez-Prelcic, S. Rangan, W. Roh, and A. M. Sayeed, "An overview of signal processing techniques for millimeter wave mimo systems," *IEEE J. Sel. Topics in Signal Process.*, vol. 10, no. 3, pp. 436–453, April 2016.

[5] O. Orhan, E. Erkip, and S. Rangan, "Low power analog-to-digital conversion in millimeter wave systems: Impact of resolution and bandwidth on performance," in *IEEE Inf Theory and App. Workshop (ITA), 2015*, Feb 2015, pp. 191–198.

[6] R. D. Taranto, S. Muppirisetty, R. Raulefs, D. Slock, T. Svensson, and H. Wymeersch, "Location-aware communications for 5G networks: How location information can improve scalability, latency, and robustness of 5G," *IEEE Signal Process. Mag*, vol. 31, no. 6, pp. 102–112, Nov 2014.

[7] N. Garcia, H. Wymeersch, E. G. Ström, and D. Slock, "Location-aided mm-wave channel estimation for vehicular communication," in *IEEE 17th Int. Workshop on Signal Process. Advances in Wireless Commun.*, July 2016, pp. 1–5.

[8] K. Witrisal, P. Meissner, E. Leitinger, Y. Shen, C. Gustafson, F. Tufvesson, K. Haneda, D. Dardari, A. F. Molisch, A. Conti, and M. Z. Win, "High-accuracy localization for assisted living: 5G systems will turn multipath channels from foe to friend," *IEEE Signal Process. Mag*, vol. 33, no. 2, pp. 59–70, March 2016.

[9] L. S. Muppirisetty, T. Svensson, and H. Wymeersch, "Spatial wireless channel prediction under location uncertainty," *IEEE Trans. on Wireless Commun.*, vol. 15, no. 2, pp. 1031–1044, Feb 2016.

[10] C. Han, X. Zhu, A. Doufexi, and T. Kocak, "Location-aided multi-user beamforming for 60 GHz WPAN systems," in *IEEE 75th Veh Technol. Conf. VTC*, May 2012, pp. 1–5.

[11] J. C. Aviles and A. Kouki, "Position-aided mm-wave beam training under NLOS conditions," *IEEE Access*, vol. 4, pp. 8703–8714, 2016.

[12] N. Akbar, S. Yan, N. Yang, and J. Yuan, "Mitigating pilot contamination through location-aware pilot assignment in massive MIMO networks," in *2016 IEEE Globecom Workshops (GC Wkshps)*, Dec 2016, pp. 1–6.

[13] S. M. Kay, *Fundamentals of Statistical Signal Processing: Estimation Theory*. NJ, USA: Prentice-Hall, Inc., 1993.

[14] J. Li, J. Conan, and S. Pierre, "Joint estimation of channel parameters for MIMO communication systems," in *2nd Int. Symp. on Wireless Commun. Systems*, Sept 2005, pp. 22–26.

[15] M. D. Larsen, A. L. Swindlehurst, and T. Svantesson, "Performance bounds for MIMO-OFDM channel estimation," *IEEE Trans. Signal Process.*, vol. 57, no. 5, pp. 1901–1916, May 2009.

[16] Y. Shen and M. Z. Win, "Performance of localization and orientation using wideband antenna arrays," in *2007 IEEE International Conference on Ultra-Wideband*, Sept 2007, pp. 288–293.

[17] ——, "On the accuracy of localization systems using wideband antenna arrays," *IEEE Trans. on Commun.*, vol. 58, no. 1, pp. 270–280, Jan 2010.

[18] ——, "Fundamental limits of wideband localization – part I: A general framework," *IEEE Trans. on Inf. Theory*, vol. 56, no. 10, pp. 4956–4980, Oct 2010.

[19] Y. Shen, H. Wymeersch, and M. Z. Win, "Fundamental limits of wideband localization – part II: Cooperative networks," *IEEE Trans. on Info Theory*, vol. 56, no. 10, pp. 4981–5000, Oct 2010.

[20] A. Shahmansoori, G. E. Garcia, G. Destino, G. Seco-Granados, and H. Wymeersch, "Position and orientation estimation through millimeter wave MIMO in 5G systems," 2017. [Online]. Available: https://arxiv.org/abs/1702.01605

[21] Y. Han, Y. Shen, X. P. Zhang, M. Z. Win, and H. Meng, "Performance limits and geometric properties of array localization," *IEEE Trans. on Inf. Theory*, vol. 62, no. 2, pp. 1054–1075, Feb 2016.

[22] A. Guerra, F. Guidi, and D. Dardari, "Single anchor localization and orientation performance limits using massive arrays: MIMO vs. beamforming," 2017. [Online]. Available: https://arxiv.org/abs/1702.01670

[23] H. Deng and A. Sayeed, "Mm-wave MIMO channel modeling and user localization using sparse beamspace signatures," in *IEEE 15th Int. Workshop on Signal Process. Advances in Wireless Commun. (SPAWC), 2014*, June 2014, pp. 130–134.

[24] H. Van Trees, *Detection, Estimation, and Modulation Theory, Optimum Array Processing. Part IV*, ser. Detection, Estimation, and Modulation Theory. Wiley, 2002.

[25] M. Fakharzadeh, M. R. Nezhad-Ahmadi, B. Biglarbegian, and J. Ahmadi-Shokouh, "CMOS phased array transceiver technology for 60 GHz wireless applications," *IEEE Trans. Antennas Propag.*, vol. 58, no. 4, pp. 1093–1104, April 2010.

[26] V. Venkateswaran and A. J. van der Veen, "Analog beamforming in MIMO communications with phase shift networks and online channel estimation," *IEEE Trans. Signal Process.*, vol. 58, no. 8, pp. 4131–4143, Aug 2010.

[27] A. N. D'Andrea, U. Mengali, and R. Reggiannini, "The modified Cramér-Rao bound and its application to synchronization problems," *IEEE Trans. on Commun.*, vol. 42, no. 234, pp. 1391–1399, Feb 1994.

[28] J. Wilkinson, "Almost diagonal matrices with multiple or close eigenvalues," *Linear Algebra and its Applications*, vol. 1, no. 1, pp. 1–12, Jan 1968.

[29] Z. Abu-Shaban, H. Wymeersch, X. Zhou, G. Seco-Granados, and T. Abhayapala, "Random-phase beamforming for initial access in millimeter-wave cellular networks," in *2016 IEEE GLOBECOM Conf.*, Dec 2016, pp. 1–6.

[30] C. Gentner, T. Jost, W. Wang, S. Zhang, A. Dammann, and U. C. Fiebig, "Multipath assisted positioning with simultaneous localization and mapping," *IEEE Trans. on Wireless Commun.*, vol. 15, no. 9, pp. 6104–6117, Sept 2016.